

Nonsynchronous interactions

V F Kravchenko, A A Kurayev, A K Sinitsyn

DOI: 10.1070/PU2007v050n05ABEH006252

Contents

1. Introduction	489
2. The band and criticality of the cyclotron-autoresonance conditions	490
3. Nonsynchronous interaction: apparent contradictions in averaged solutions	493
4. Nonsynchronous interaction of a relativistic electron flow with the rotating E_{11n} field of a cylindrical resonator	496
5. Coaxial oscillator with a nonsynchronous interaction	499
6. The effect of nonsynchronous azimuthal spatial harmonics on the peniotron efficiency	503
7. Nonsynchronous interaction of relativistic electron flows with the fields of irregular waveguides in superpower microwave electronic devices	506
7.1 Self-consistent equations of a nonlinear model of a relativistic BWT and O-type TWT with a slow-wave structure in the form of a corrugated waveguide; 7.2 Special features of calculations of supercritical waves	
References	510

Abstract. The importance of nonsynchronous (nonresonant) forces is demonstrated using the interaction of electron flows with regular and irregular electrodynamic structures as an example. These forces lead to cumulative ‘nonsynchronous-interaction’ effects, which manifest themselves both without and in the presence of synchronous (resonant) interaction.

1. Introduction

In modern physics, although the performance of available computers has substantially increased, the formulation of mathematical models of some investigated phenomena or experimental setups still requires neglecting a number of factors that are assumed to have no significant effect on the characteristics of the phenomenon or setup (and, anyway, all factors cannot obviously be taken into account). Such factors are typically related to nonresonant or nonsynchronous forces or interactions. At first glance, this is correct and reasonable: in contrast to synchronous interactions, these should seemingly have no cumulative effects because their action should not be significant, on average. However, as we show here, this is not the case, in some particular foreknown cases at least.

(1) Obviously, these are cases without synchronous (resonant) interactions, with the presence of only a nonsynchronous (nonresonant) component of the forces. The nonlinear nature of the process gives rise to quadratic terms that are responsible for the origin of a systematic (cumulative) component of the interaction.

(2) There may be a situation where the resonant (synchronous) effects of the interaction are mutually balanced, and hence the nonsynchronous interaction acquires a primary role. As an example, we note the interaction between a helical electron flow, controlled by a uniform magnetic field, and a T wave. If there is a synchronism (cyclotron resonance) between the electrons and a forward or backward wave, the phenomenon of autoresonance occurs: the relative phase in the wave does not vary because of the exact balance between the phase changes due to relativistic azimuthal displacements of the electron and its inertial longitudinal displacements [1, 2]. However, such a mechanism is possible only if the electron flow is in synchronism (cyclotron resonance) with an isolated, constant-amplitude T wave running concurrently with or oppositely to the flow. In reality, this case is impossible, because the electron flow emits both a forward and a backward wave. Therefore, a nonsynchronous forward or backward wave arises, and its interference with the synchronous forward or backward wave, respectively, violates the balance between the azimuthal and longitudinal bunchings in the electron flow, such that positive effects — either amplification (a synchronous forward wave) or generation (a backward wave) — become possible in the T-field [3, 4]. In other words, if the nonsynchronous interaction with the forward or backward wave excited by the flow is not taken into account, the erroneous conclusion can be made that phase bunching and, accordingly, energy exchange between the helical electron flow and the T waves are impossible.

(3) This is also the case if the nonsynchronous interaction substantially affects the fundamental (resonant) effects, for

V F Kravchenko Institute of Radio Engineering and Electronics, Russian Academy of Sciences
Mokhovaya ul. 11, korp. 7, 125009 Moscow, Russian Federation
Tel.: (7-495) 203 47 93

E-mail: kravchenko_vf@fromru.com

A A Kurayev, A K Sinitsyn Belarussian State University of Information Science and Radio Engineering
ul. P Brovki 6, 220013 Minsk, Belarus
Tel.: (375-17) 293 84 98, 293 23 46

E-mail: kurayev@bsuir.by, sinitsin@cosmostv.by

Received 13 October 2006

Uspekhi Fizicheskikh Nauk 177 (6) 511 – 534 (2007)

Translated by A V Getling; edited by A M Semikhatov

example, the nonsynchronous spatial harmonics affect the interaction of electrons with electromagnetic fields.

We here demonstrate the role of nonsynchronous interactions using the interaction between electrons and electromagnetic fields as an example, according to the authors' research interests. However, we can conjecture that the nonsynchronous interactions of other types play a similar role, and therefore they should be taken into account or, at least, their effects should be estimated.

2. The band and criticality of the cyclotron-autoresonance conditions

The content of this section is based on the material in Ref. [5]. The phenomenon of the cyclotron autoresonant motion of a charged particle in the field of a T wave propagating along the direction of a constant magnetic field was first described and investigated in Refs [1, 2]. This phenomenon consists in the fact that a charged particle, irrespective of its acceleration or deceleration due to the field, moves exactly along the helical constant-phase line of a resonant, circularly polarized component of a T wave. In other words, the relative phase of the charged particle (from here on, electron) in the field of a T wave remains invariable, although the particle energy varies. Therefore, if the electrons enter the interaction region at a braking phase of the wave field, they are continuously decelerated over a long path until they fully stop; the length of this path is determined only by the initial phase of the T wave, its amplitude, and the energy of the electron. These properties of the cyclotron autoresonance turned out to be very attractive in terms of using such regimes in the devices of relativistic electronics: cyclotron-resonance masers [6–13], peniomagnetrons [14], and gyrotrons [15–17]. It is expected that using the autoresonant regime will allow substantially enhancing the efficiency of relativistic generators and amplifiers and even bringing it closer to its maximum achievable value with a simultaneous increase in the working frequency.

Experiments on cyclotron-autoresonance masers (CARMs) with extended interaction [18–20] revealed a strong disagreement with theoretical expectations [6–13]: efficiencies of 2–4% were actually obtained instead of the 20–40% predicted. We note in passing that a wrong expression for the 'one-particle' efficiency was used in the above-mentioned theoretical studies [6–13]; it contradicts the integral of motion of an electron in a running wave at $v_{ph} \neq c$ [20]. However, the main source of this discrepancy is most likely in the criticality of the autoresonance conditions, which increases dramatically as the length of the interaction region increases; this was already noted long ago in [15]. A nonoptimal choice of the electron-beam pitch factor in experiments [18–20] resulted in a sharp decrease in efficiency. An analytic solution of the equation of motion of a charged particle in the field of a T wave under strictly autoresonant conditions was obtained in [1]. We here obtain analytic solutions also for a nonresonant case, which allows investigating autoresonance as a physical phenomenon in various situations: at a fixed length of the interaction region, at a fixed amplitude of the wave, at a given number of circuits of the particle trajectory, etc. Such studies enable estimating the band and criticality of the cyclotron-autoresonance conditions at varying parameters of the electron beam and varying conditions of the interaction, which appears to be useful for choosing the type and arrangement of the devices of

relativistic electronics that operate in nearly autoresonant regimes.

The equations of motion of an electron in a given rotating T-field of a resonator and a uniform magnetic field, with the action of the backward nonsynchronous component of the resonator standing field and of the nonsynchronous left-hand polarized component neglected, are given by [1, 21]

$$\frac{d\gamma\boldsymbol{\beta}}{d\theta} = -A\left\{\mathbf{E} + [\boldsymbol{\beta} [\mathbf{z}_0 \mathbf{E}]]\right\} - F_0 [\boldsymbol{\beta} \mathbf{z}_0], \quad (1)$$

$$\frac{dx}{d\theta} = \beta_x, \quad \frac{dy}{d\theta} = \beta_y, \quad \frac{dz}{d\theta} = \beta_z, \quad (2)$$

where

$$\theta = \omega t, \quad A = \frac{eE'_m}{m_0\omega c}, \quad F_0 = \frac{eB_0}{m_0\omega},$$

$$\boldsymbol{\beta} = \frac{\mathbf{v}}{c}, \quad \gamma = \frac{1}{\sqrt{1 - \boldsymbol{\beta}^2}}, \quad \mathbf{x} = \frac{\omega}{c} \mathbf{x} = x \mathbf{x}_0 + y \mathbf{y}_0 + z \mathbf{z}_0.$$

Based on the hyperresonance conditions, we choose the right-hand polarized T wave

$$\mathbf{E} = \cos(\theta - z + \psi_0) \mathbf{x}_0 + \sin(\theta - z + \psi_0) \mathbf{y}_0. \quad (3)$$

The initial conditions for system (1), (2) are

$$\begin{aligned} \theta = 0, \quad z = 0, \quad \beta_z(0) = \beta_{\parallel}, \quad \beta_x(0) = \beta_{\perp} \cos \psi_0, \\ \beta_y(0) = \beta_{\perp} \sin \psi_0, \quad x(0) = 0, \quad y(0) = 0. \end{aligned} \quad (4)$$

The electronic efficiency of the interaction can be calculated from the change in the relativistic mass factor $\eta(z)$ as

$$\eta(z) = \frac{\gamma_0 - \gamma(z)}{\gamma_0 - 1}, \quad \gamma_0 = \gamma(0). \quad (5)$$

To obtain an analytic solution, we transform Eqn (1) following a line similar to that described in Ref. [1]. We take the scalar product of Eqn (1) with $\boldsymbol{\beta}$ to obtain the well-known equation for γ ,

$$\frac{d\gamma}{d\theta} = -A\boldsymbol{\beta} \mathbf{E}. \quad (6)$$

The scalar multiplication of Eqn (1) by \mathbf{z}_0 with the use of Eqn (6) yields the integral of motion

$$\gamma(1 - \beta_z) = k_0 = \text{const} = \gamma_0(1 - \beta_{z0}), \quad (7)$$

where γ_0 and β_{z0} are the values of γ and β_z at the inlet of the resonator. We introduce the transverse vector $\boldsymbol{\beta}_t = \beta_x \mathbf{x}_0 + \beta_y \mathbf{y}_0$ and use Eqns (1), (6), and (7) to derive the equation

$$\frac{d\gamma\boldsymbol{\beta}_t}{d\theta} = -(1 - \beta_z) \left\{ A\mathbf{E} + \frac{F_0}{k_0} [\gamma\boldsymbol{\beta}_t \mathbf{z}_0] \right\}.$$

Next, we pass to the new independent variable $\Phi = \theta - z$. Using the notation $\mathbf{P}_t = \gamma\boldsymbol{\beta}_t$, we write the following linear equation for the transverse component of the momentum \mathbf{P}_t with a harmonic right-hand side:

$$\frac{d\mathbf{P}_t}{d\Phi} + \frac{F_0}{k_0} [\mathbf{P}_t \mathbf{z}_0] = -A\mathbf{E}(\Phi). \quad (8)$$

We note that Eqn (8) is valid for an arbitrarily polarized T wave and F_0 of an arbitrary sign. To obtain the exact solution of Eqn (8), it is convenient to write it in complex form. For this, we introduce the notation

$$\dot{P}_t = P_x + jP_y,$$

$$\dot{E} = \cos(\Phi + \psi_0) + j \sin(\Phi + \psi_0) = \exp(j\Phi) \exp(j\psi_0).$$

We then have

$$\begin{aligned} \frac{d\dot{P}_t}{d\Phi} - j \frac{F_0}{k_0} \dot{P}_t &= -A \exp(j\psi_0) \exp(j\Phi), \\ \dot{P}_t(0) = \dot{P}_{t0} = P_{x0} + jP_{y0} &= |\dot{P}_{t0}| \exp(j\psi_p), \end{aligned} \quad (9)$$

where $\Phi > 0$, and θ and z are measured from the resonator inlet.

We represent the exact solution of problem (9) as follows:
(a) $F_0/k_0 \neq 1$ (nonresonant motion),

$$\begin{aligned} \dot{P}_t &= \dot{P}_{t0} \exp\left(j \frac{F_0}{k_0} \Phi\right) \\ &\quad - \frac{jA \exp(j\psi_0)}{1 - F_0/k_0} \left[\exp\left(j \frac{F_0}{k_0} \Phi\right) - \exp(j\Phi) \right]; \end{aligned} \quad (10)$$

(b) $F_0/k_0 = 1$ (autoresonant motion),

$$\begin{aligned} \dot{P}_t &= [\dot{P}_{t0} - A \exp(j\psi_0) \Phi] \exp(j\Phi) \\ &= [|\dot{P}_{t0}| \exp(j\psi_p) - A\Phi \exp(j\psi_0)] \exp(j\Phi). \end{aligned} \quad (11)$$

Expressions (10) and (11) were obtained for the transverse component of the momentum. To determine its longitudinal component $P_z = \gamma\beta_z$, we use integral of motion (7) and the relation $\gamma^2 = 1 + P_x^2 + P_y^2 + P_z^2$. Then,

$$P_z = \gamma(z) - k_0, \quad \gamma = \frac{1 + P_x^2 + P_y^2 + k_0^2}{2k_0}, \quad (12)$$

where $|\dot{P}_t|^2 = P_x^2 + P_y^2$, which is involved in the expression for γ , has the following forms:

(a) in the case of nonresonant motion ($\alpha = 1 - F_0/k_0$),

$$\begin{aligned} |\dot{P}_t|^2 &= |\dot{P}_{t0}|^2 + \frac{2A^2}{\alpha^2} (1 - \cos \alpha\Phi) \\ &\quad - 4 \frac{|\dot{P}_{t0}| A}{\alpha} \sin \frac{\alpha\Phi}{2} \cos \left(\frac{\alpha\Phi}{2} + \psi_0 - \psi_p \right), \end{aligned} \quad (13)$$

(b) in the case of autoresonant motion ($\alpha = 0$),

$$P_x^2 + P_y^2 = |\dot{P}_{t0}|^2 + A^2\Phi^2 - 2|\dot{P}_{t0}| A\Phi \cos(\psi_0 - \psi_p). \quad (14)$$

To solve Eqns (2), we introduce the notation $\dot{r} = x + jy$ and, using relation (7) and passing to the independent variable Φ , write the equations

$$\frac{d\dot{r}}{d\Phi} = \frac{\dot{P}_t}{k_0}, \quad \dot{r}(0) = \dot{r}_0, \quad \frac{dz}{d\Phi} = \frac{P_z}{k_0} = \frac{\gamma - k_0}{k_0}, \quad z(0) = 0. \quad (15)$$

After the substitution of expressions (10)–(14) in Eqn (15), we obtain the exact solutions for $\dot{r}(\Phi)$ and $z(\Phi)$.

We now find the solution of Eqns (15) in the case of autoresonant motion. We use expression (11) for \dot{P}_t in Eqn (15) and obtain, upon integration,

$$\begin{aligned} \dot{r} &= \dot{r}_0 + \frac{1}{F_0} [A \exp(j\psi_0) + j\dot{P}_{t0}] \\ &\quad - \frac{1}{F_0} [A \exp(j\psi_0) + j\dot{P}_{t0} - jA\Phi \exp(j\psi_0)] \exp(j\Phi). \end{aligned} \quad (16)$$

Using Eqns (12) and (14), we write the equation for the variable z that enters Eqn (15) in the form

$$\frac{dz}{d\Phi} = \frac{1 - k_0^2 + (P_{x0} - A\Phi \cos \psi_0)^2 + (P_{y0} - A\Phi \sin \psi_0)^2}{2k_0^2}. \quad (17)$$

Integrating Eqn (17) yields the equation that relates Φ and z :

$$z = a\Phi^3 + b\Phi^2 + c\Phi, \quad (18)$$

where

$$\begin{aligned} a &= \frac{A^2}{6k_0^2}, \\ b &= -A \frac{P_{x0} \cos \psi_0 + P_{y0} \sin \psi_0}{2k_0^2}, \\ c &= \frac{1 - k_0^2 + P_{x0}^2 + P_{y0}^2}{2k_0^2}. \end{aligned}$$

Similar but more cumbersome relations can be obtained in the nonresonant case (10):

$$\begin{aligned} z &= \frac{1}{2k_0^2} \left\{ (1 - k_0^2 + |\dot{P}_{t0}|^2) \Phi + \frac{2A^2}{\alpha^3} (\alpha\Phi - \sin \alpha\Phi) \right. \\ &\quad - \frac{2|\dot{P}_{t0}| A}{\alpha^2} [\cos(\psi_0 - \psi_p) - \cos(\alpha\Phi + \psi_0 - \psi_p) \\ &\quad \left. - \alpha\Phi \sin(\psi_0 - \psi_p)] \right\}. \end{aligned} \quad (19)$$

Given the initial conditions at the inlet of the resonator, expressions (11)–(19) determine the motion of the electron interacting with the backward partial T wave at any section z . Figure 1a presents a family of functions $\eta(F_0)$ at $A = 0.015$ and various β_0 . For any β_0 , the length of the interaction region L and the pitch factor $q = v_{\perp}/v_{\parallel} = \sqrt{2/(\gamma_0 - 1)}$ were chosen based on the condition of the full stop of the electron at the end of this region in the case of exact autoresonance ($F_0 = 1$), i.e., $\eta(1) = 1$. The appearance of the resonant curves is highly specific: in contrast to the case of normal resonance, the point of exact autoresonance is not stationary, i.e., the first derivative $\eta'(F_0)$ has a discontinuity at this point. Then, $\eta'(1 - 0) = -\eta'(1 + 0)$, and the derivatives themselves are very large, which testifies to the criticality of the optimum conditions for autoresonance. The band of autoresonance is fairly narrow and narrows as the relativism of the electrons, β_0 , increases. This can easily be understood because for a fixed amplitude A , the length of the optimum region decreases with the increase in β_0 , which naturally narrows the autoresonance band.

The ‘resonance’ curves $\eta(q)$ for $F_0 = 1$, $A = 0.015$, and given β_0 (i.e., γ_0) shown in Fig. 1a characterize the criticality of the autoresonance conditions with respect to departures of

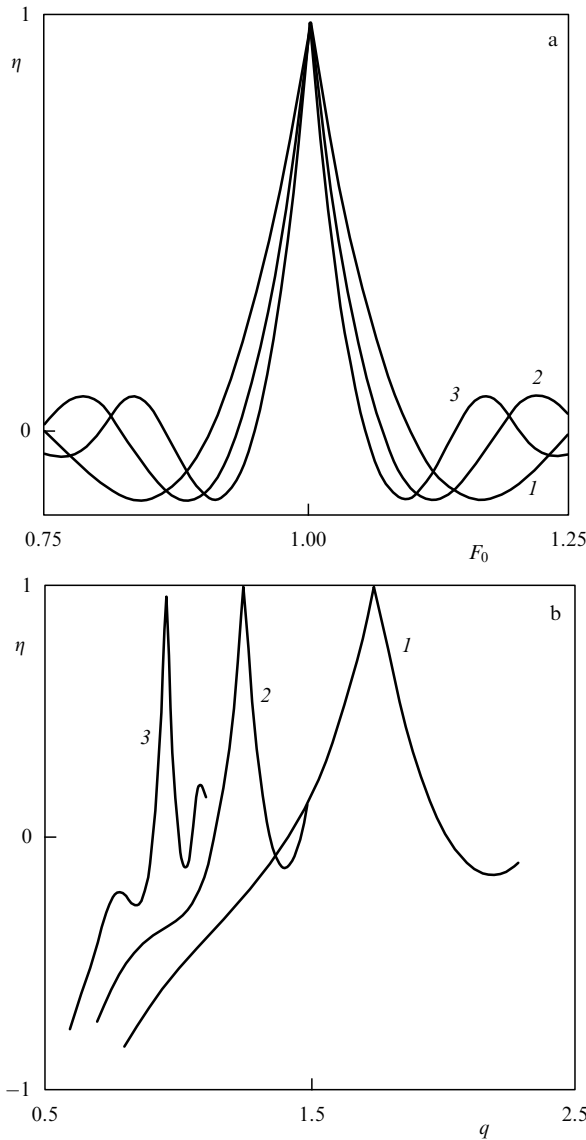


Figure 1. Resonance curves for the fixed $A = 0.015$: (a) $\eta(F_0)$, (b) $\eta(q)$; 1 — $\beta_0 = 0.8$, $L = 17.1$, $\Phi = 77.0$; 2 — $\beta_0 = 0.9$, $L = 46.3$, $\Phi = 107.2$; 3 — $\beta_0 = 0.95$, $L = 102.7$, $\Phi = 139.9$.

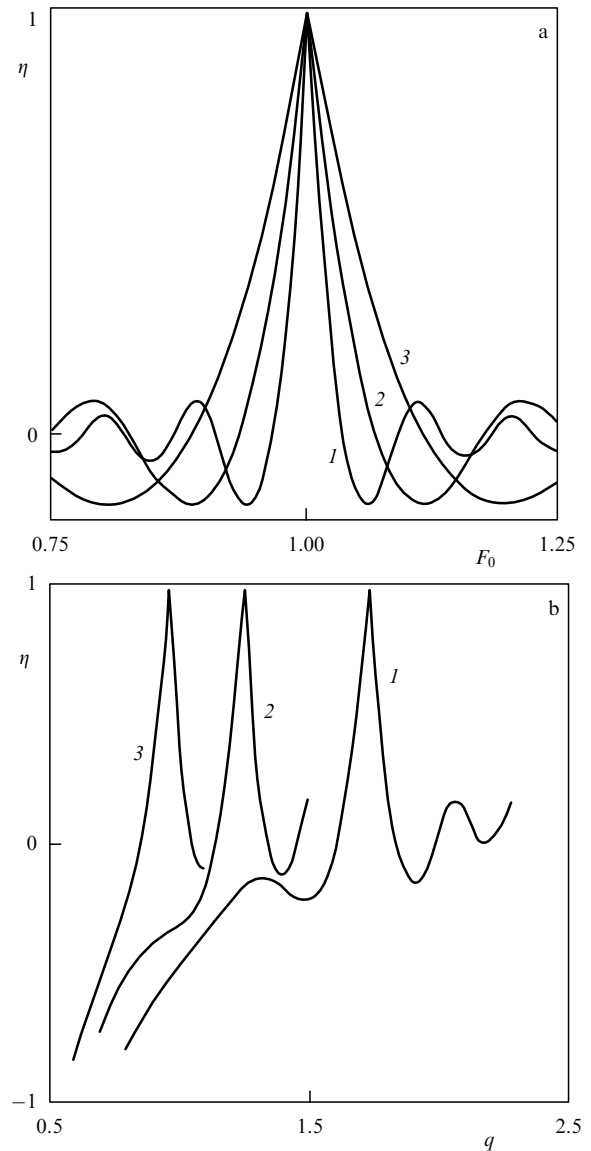


Figure 2. Resonance curves for the fixed $L = 15\pi$: (a) $\eta(F_0)$, (b) $\eta(q)$; 1 — $\beta_0 = 0.8$, $A = 0.0055$, $\Phi = 211.7$; 2 — $\beta_0 = 0.9$, $A = 0.0147$, $\Phi = 109.2$; 3 — $\beta_0 = 0.95$, $A = 0.0327$, $\Phi = 64.2$.

the beam parameters (pitch factor q) from the optimum values computed based on the condition of the full removal of the electron energy in the case of exact autoresonance [$\gamma_0(1 - \beta_{z0}) = 1$]. The criticality of $\eta(q)$ at the optimum points increases dramatically with the increase in β_0 . To a certain extent, this is due to the above-mentioned factor, the increase in the optimum length of the interaction region at a given A . In addition, the optimum condition itself, $1 - \beta_{z0} = \gamma_0^{-1}$, becomes more critical as γ_0 increases.

Figure 2a represents a family of resonance curves $\eta(F_0)$ for the interaction region length $L = 15\pi$ and various β_0 . As in the preceding case, the choice of A and q was based on the condition $\eta(1) = 1$. The functions $\eta(F_0)$ are similar to those shown in Fig. 1a; however, the β_0 dependence in the family $\eta(F_0)$ is here exactly the opposite: now, the resonance band broadens as β_0 increases. This can easily be understood, because now, given the length of the interaction region, the number of cyclotron circuits of the electron decreases and the resonance band broadens with an increase in $\eta(q)$. Figure 2b

shows a family of dependences $\eta(q)$ for $F = 1$, $L = 15\pi$, and varying β_0 . Compared to the analogous family in Fig. 1b, the general pattern of dependences is preserved and, importantly, the criticality of $\eta(q)$ still increases with increasing β_0 , although not so sharply as in the previous case. Thus, the requirements for the quality of the electron flow (the minimum spread in q) and for q complying with the condition of the full removal of the electron energy [$\gamma_0(1 - \beta_{z0}) = 1$] become more stringent as the relativism of the beam is increased.

Shown in Fig. 3a is a family of resonant curves $\eta(F_0)$, with $N = 10$ circuits of the electron in the interaction region, for varying β_0 . As follows from Fig. 3a, this family degenerates into a single curve $\eta(F_0)$ for all β_0 values; i.e., given N , the resonant curves $\eta(F_0)$ are β_0 -independent. Figure 3b presents a family of dependences $\eta(q)$ at $F_0 = 1$, $N = 10$, and varying β_0 . The general pattern of the dependences remains similar to those shown in Figs 1b and 2b: the criticality of $\eta(q)$ increases fairly rapidly as β_0 decreases.

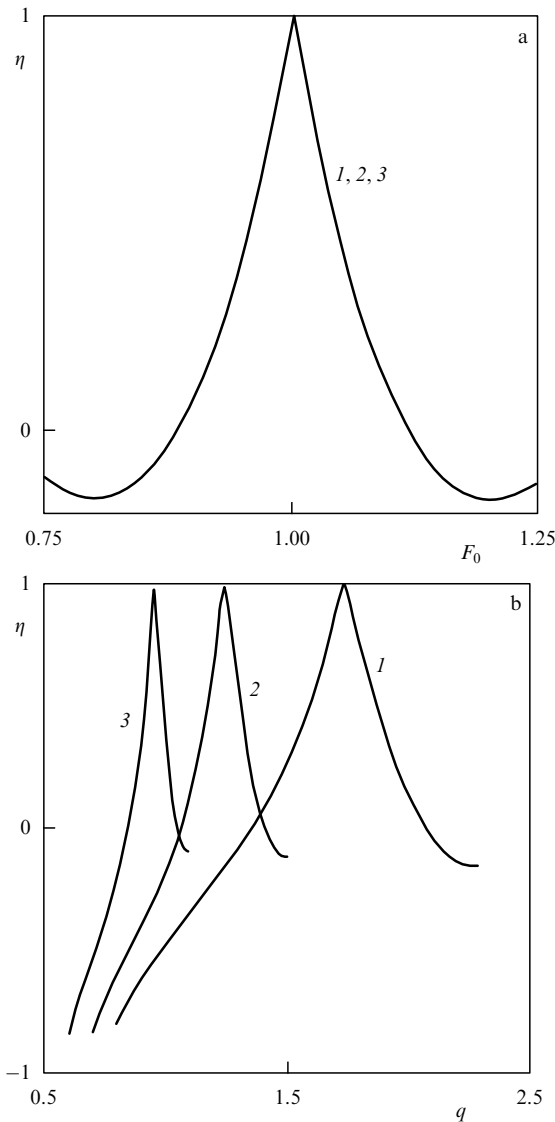


Figure 3. Resonance curves for the fixed $\Phi = 20\pi$ ($N = 10$): (a) $\eta(F_0)$, (b) $\eta(q)$; 1 — $\beta_0 = 0.8$, $A = 0.0184$, $L = 13.9$; 2 — $\beta_0 = 0.9$, $A = 0.0256$, $L = 27.10$; 3 — $\beta_0 = 0.95$, $A = 0.0334$, $L = 46.13$.

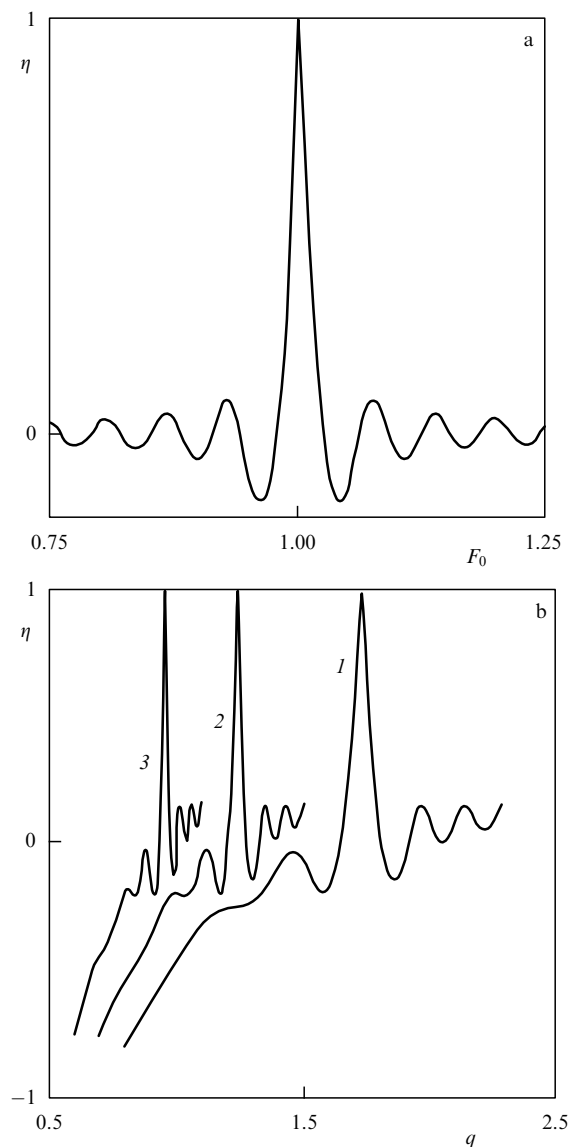


Figure 4. Resonance curves for the fixed $\Phi = 100\pi$ ($N = 50$): (a) $\eta(F_0)$, (b) $\eta(q)$, 1 — $\beta_0 = 0.8$, $A = 0.0037$, $L = 69.8$; 2 — $\beta_0 = 0.9$, $A = 0.0051$, $L = 135.5$; 3 — $\beta_0 = 0.95$, $A = 0.0067$, $L = 230.6$.

Figures 4a and 4b show the dependences $\eta(F)$ and $\eta(q)$, similar to the preceding ones for $N = 50$ and various β_0 . It follows from these dependences that the resonance band substantially narrows here and the criticality of the resonance conditions increases. The criticality of $\eta(q)$ is enhanced very sharply with increasing β_0 . Therefore, the difficulties associated with developing high-efficiency CARMs becomes understandable: to achieve an appropriate bunching of electrons as $\beta_{ph} \rightarrow 1$ (e.g., $\beta_{ph} = 1.03$ [11]), a long interaction region (or, more precisely, large N) is needed; however, as N is increased, the criticality of a CARM with respect to the deviations in the beam parameters (most of all, q) forming the optimum values increases dramatically, especially at high β_0 , according to the above results. At the same time, precisely ultrarelativistic CARMs seem to be interesting in view of the possibility of increasing the working frequency proportionally to γ^2 [11]. These contradictions can likely be resolved only in cascade CARMs, where the first cascade operates at $\beta_{ph} \approx 1.5-2$, ensuring the necessary phase bunching of electrons, while the second one (the remover) operates in the

CARM regime at $\beta_{ph} \approx 1$ (with a high quality of the electron beam and with a strict correspondence of its parameters to the condition of full energy removal) and ensures a high efficiency of the device.

3. Nonsynchronous interaction: apparent contradictions in averaged solutions

The content of this section is based on Ref. [22]. In closing the tenth lecture (Prospects) of his course “Foundations of SuperHigh-Frequency Electronics” [23], L A Vainshtein gave principal attention to the nonsynchronous interaction of electrons with a fast oscillating field. This interaction is remarkable in that an electron in a nonuniform (in the direction of the initial velocity of the electron) field acquires an increment in the systematic component of its velocity. This effect is similar to that discovered by Kapitza [24] in the behavior of a pendulum with a vibrating suspension. This phenomenon in electronics was discovered and investigated by Miller [25, 26]. As the instrument of investigation, an

averaging technique was used in the equation of motion for the electron in the ‘*t*’ system. The averaging technique was applied again 20 years later to the equations of motion of an electron in a nonuniform high-frequency field [27]; however, the ‘*t*’ system was used for the equations in one case and the ‘*z*’ system was used in another. Accordingly, the right-hand sides of the equation for the systematic component of the acceleration in these two cases proved to be equal in absolute value but opposite in sign. The apparent insolubility of this contradiction led the authors of Ref. [27] to the conclusion that no systematic velocity increase is possible or this effect is weak and cannot therefore be isolated, i.e., Miller’s effect does not exist and the electron is not reflected by an increasing field. We demonstrate below that this conclusion is not correct, although the ‘contradiction’ noted in Ref. [27] is actually present. The substantial difference between the descriptions of the electron motion in the ‘*t*’ and ‘*z*’ systems plays a decisive role here.

Let a rectilinear nonrelativistic electron flow directed along the *z* axis interact with the *z* component of a given electric field at a frequency ω , $E_z = E(z) \cos(\omega t + \varphi)$. The interaction interval is $0 \leq z \leq L$. The process of interaction between the electron flow and the electromagnetic field can be studied by analyzing the collective interaction between a high-frequency (HF) field and an *N*-particle ensemble originally distributed uniformly with respect to the electronic wavelength $\lambda_{\omega} = 2\pi v_0/\omega$. All particles of the ensemble enter the interaction region one by one over one oscillation period at an initial velocity v_0 . If the interaction of particles, i.e., electrons, is ignored, the motion of each of them in the interaction region is described by the equation (in the nonrelativistic approximation)

$$\frac{d^2 z'_i}{dt^2} = \frac{e}{m_0} E(z'_i) \cos(\omega t + \varphi_i), \quad (20)$$

where z'_i is the dimensional coordinate of the *i*th electron, φ_i is the phase at which it enters the interaction region, and e and m_0 are the charge and rest mass of the electron.

Next, we pass to the dimensionless variables

$$z_i = \frac{z'_i}{L}, \quad V_i = \frac{v_i}{v_0}, \quad \tau = \frac{v_0 t}{L}, \quad E(z') = E_m f\left(\frac{z'}{L}\right),$$

$$A = \frac{e E_m L}{m_0 v_0^2}, \quad \theta_0 = \frac{\omega L}{v_0}.$$

We can then rewrite Eqn (20) as the system of equations

$$\frac{dV_i}{d\tau} = A f(z_i) \cos(\theta_0 \tau + \varphi_i),$$

$$\frac{dz_i}{d\tau} = V_i. \quad (21)$$

The initial conditions for system (21) are specified in the form

$$V_i(0) = 1, \quad z_i(0) = 0, \quad \varphi_i = \frac{2\pi i}{N}. \quad (22)$$

We note that because the interaction interval is fixed, $f(z_i) \equiv 0$ in Eqn (20) at $z_i \leq 0$ and $z_i \geq 1$. If Eqns (21) are written in the ‘*t*’ system, this fact is important in analyzing the state resulting from the motion of the electron in the field over a finite interval (at $z = 1$ or at a current z). Specifically, we need to compute a τ_i at which the electron finds itself at z or $z = 1$. This recalculation procedure can be avoided if the

equations of motion for the electron are originally written in the ‘*z*’ system,

$$\frac{dV_i}{dz} = \frac{A f(z)}{V_i} \cos(\theta_0 \tau_i + \varphi_i),$$

$$\frac{d\tau_i}{dz} = \frac{1}{V_i}, \quad (23)$$

$$V_i(0) = 1, \quad \tau_i(0) = 0, \quad \varphi_i = \frac{2\pi i}{N}.$$

This system of equations, being computationally simpler (although more complex in terms of the interpretation of the results), is unfortunately not universal, in contrast to the ‘*t*’ system. It allows studying the motion of the electron only for $V_i > 0$, i.e., up to the point where the electron stops (and hence its total, systematic + oscillating velocity vanishes). Thus, neither the reflection of the electron nor its earlier stages of motion (with zero total V_i) can be analyzed in the ‘*z*’ system. The power of the interaction between the electron flow of power P_0 and the electromagnetic field in the ‘*z*’ and ‘*t*’ systems can be calculated using the formulas

$$\frac{P(z)}{P_0} = \frac{2A}{N} \sum_{i=1}^N \int_0^z f(z) \cos(\theta_0 \tau_i(z) + \varphi_i) dz$$

$$= \frac{2A}{N} \sum_{i=1}^N \int_0^{\tau_{iz}} V_i(\tau) f(z_i(\tau)) \cos(\theta_0 \tau + \varphi_i) d\tau, \quad (24)$$

$$z_i(\tau_{iz}) = z.$$

The problem in (21), (22) or (23) can be solved using modern PCs to any preassigned accuracy, which allows finding the entire pattern of the one-dimensional, nonsynchronous interaction of electrons with a uniform electric field for particular functions $f(z)$. Our aim is, however, to check the reliability of the conclusions in Refs [23, 25, 26] and to understand the essence of the contradiction noted in Ref. [27] using the exact solutions. In those studies, solutions were obtained using the averaging technique (whose various modifications yield the same averaged equations in the problem under consideration). We therefore recall the form of the solution to which the averaging technique leads.

(1) For problem (21), (22) [23, 25–27],

$$z_i = z_{ci}(\tau) + A f(z_{ci}) \cos(\theta_0 \tau + \varphi_i),$$

$$V_i = V_{ci}(\tau) - A f(z_{ci}) \frac{\sin(\theta_0 \tau + \varphi_i)}{\theta_0},$$

$$\frac{dV_{ci}}{d\tau} = -\frac{A^2}{4\theta_0^2} \frac{df^2(z_{ci})}{dz},$$

$$\frac{dz_{ci}}{d\tau} = V_{ci}, \quad (25)$$

where the subscript ‘*s*’ denotes the systematic parts of the quantities.

(2) For problem (23), with the same general form of the solution as found in Ref. [27],

$$\frac{dV_{ci}}{dz} = \frac{A^2}{4\theta_0^2 V_{ci}} \frac{df^2(z_{ci})}{dz},$$

$$\frac{d\tau_i}{dz} = \frac{1}{V_{ci}}. \quad (26)$$

At first glance, the contradiction between Eqns (25) and (26) is apparent.

We choose $f(z) = Az^2$, because the truncation used in Vainshtein's technique,

$$f(z_c + z_v) = f(z_c) + \frac{df(z_c)}{dz} z_v + \frac{1}{2} \frac{d^2f(z_c)}{dz^2} z_v^2 + O(z_v^3)$$

(with $z = z_c(\tau) + z_v(\tau)$, where $z_v(\tau)$ is the oscillating part), is exact in this case. We calculate the efficiency of the interaction between the electron ensemble and the electromagnetic field as the respective electron and wave efficiencies η_e and η_v averaged over the ensemble, as follows:

(1) in the 'z' system,

$$\eta_e(z) = \frac{\Delta W_k(z)}{W_k(0)} = 1 - \overline{V^2}, \quad \overline{V^2}(z) = \frac{1}{N} \sum_{i=1}^N V_i^2(z), \quad (27)$$

$$\eta_v(z) = \frac{P(z)}{P_0} = \frac{2A}{N} \sum_{i=1}^N \int_0^z f(z) \cos(\theta_0 \tau_i + \varphi_i) dz; \quad (28)$$

(2) in the 't' system,

$$\eta_e(z) = 1 - \frac{1}{N} \sum_{i=1}^N V_i^2(\tau_{iz}), \quad z = z_i(\tau_{iz}), \quad (29)$$

$$\eta_v(z) = \frac{2A}{N} \sum_{i=1}^N \int_0^{\tau_{iz}} V_i(\tau) f(z_i(\tau)) \cos(\theta_0 \tau + \varphi_i) d\tau. \quad (30)$$

At $N = 1$, formulas (27)–(30) define the 'individual' efficiencies η_{ei} and η_{vi} . The accuracy of the calculations can be checked by comparing $\eta_v(z)$ and $\eta_e(z)$. The limited length of this paper does not allow us to use all numerical and graphic materials obtained in comparing the exact and the averaged solutions, and we therefore present only some of them, which generally characterize the essence of the problem.

Figure 5 illustrates typical z dependences of the averaged and individual parameters of the interaction for an ensemble of eight electrons ($N = 8$) with

$$\overline{V} = \frac{1}{N} \sum_{i=1}^N V_i(z),$$

and $V_{ci}(z)$ and $\eta_{eic}(z)$ being the systematic components of V_i and η_{ei} ; they can be determined numerically using the filtration procedure. The parameters are chosen such that the applicability condition of the 'z' system ($V_i > 0$) is satisfied for all electrons everywhere to the boundary of the interaction region. The slight increase in A to 33.5 violates this condition. These data were obtained by numerically solving problem (23). As the first conclusion, we note that $\eta_e(z)$ and $\eta_{eic}(z)$ coincide for all initial phases of the i th electrons the same also applies to both \overline{V} and V_{ci} . Therefore, instead of implementing the filtration procedure for the regime with $V_i > 0$, we can simply calculate η_e and \overline{V} for the ensemble (averaging the oscillations over the ensemble). The second (and most important) conclusion is in the fact that $V_{ci}(z)$ increases in the considered regime ($V_i > 0$), which corresponds to representations (26) [and, as we see in what follows, also to representation (25)]. Accordingly, η_e and η_{eic} are negative and increase monotonically in their absolute values (which corresponds to energy pumping into the electron flow).

Figure 6a shows the dependences $\eta_e(A)$ and $\overline{V}(A)$ (at $z = 1$, for the same ensemble). The calculations were done in the 't' system for problem (21), (22), recalculating the integral

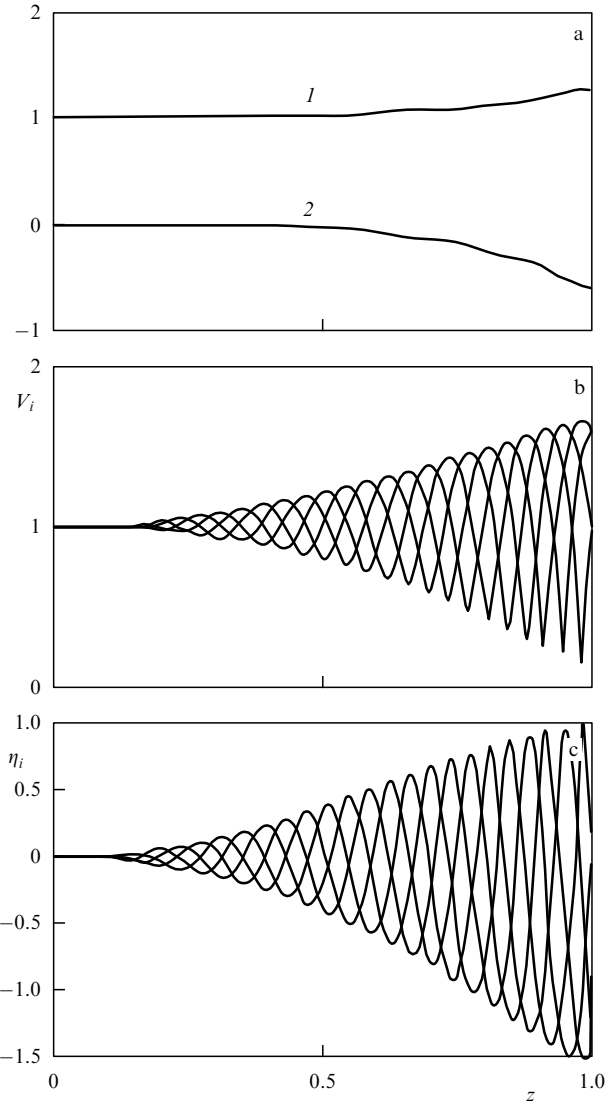


Figure 5. Characterization of the interaction of the eight-electron ensemble at $\theta_0 = 40$ and $A = 32$: (a) averaged and systematic components (curve 1 corresponds to coinciding \overline{V} and V_{ci} and curve 2 to coinciding η_e and η_{eic}); (b, c) individual trajectories, $i = 1, 3, 5, 7$.

quantities into the 'z' system. This step yielded the following information:

(1) at the point $A = 32$, the quantities $\eta_e(A)$ and $\overline{V}(A)$ exactly correspond to $\eta_e(1)$ and $\overline{V}(1)$ in Fig. 5, i.e., the computations in the 't' and 'z' systems yield exactly the same results, as could be expected;

(2) at $A \cong 59$, a decrease in \overline{V} begins (from the initial value), while η_e vanishes at this point. Near this point, the first electron that was expelled backward through $z = 0$ appears;

(3) at $A_0 \geq 59$, the quantity η_e becomes positive, and the efficiency reaches 48% at $A_0 = 60.5$. In this regime, a part of the electrons overcome the interaction interval, while another part is expelled backward;

(4) at $A = A^* \cong 62$, all electrons are reflected by the HF field, with $\overline{V}(0) = -1$ and $\eta_e(A^*) = 0$. Therefore, the inferences by Miller are quite correct at such A^* .

Finally, we can also easily check the solutions based on averaged equation (25) with a recalculation into the 'z' system and in accordance with Eqns (22). These solutions are shown with the dashed curve in Fig. 6a.

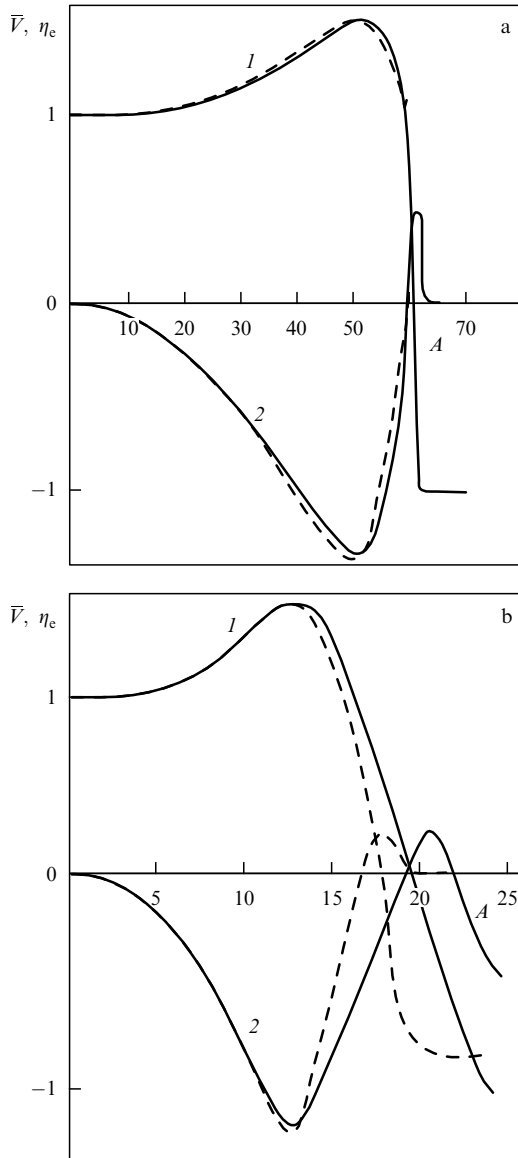


Figure 6. Integral parameters of the interaction between the electron flow and the oscillating field as a function of the amplitude A , for $\theta_0 = 40$ (a) and 10 (b). Curve 1, \bar{V} ; 2, η_e . Solid curve, full equations; dashed curve, averaged equations.

Therefore, we can state the following:

(1) the solutions of the averaged equations virtually coincide with the exact solutions;

(2) averaged equations (25) yield the same results at $A < 32$ as Eqns (26), although the sign in the equation for $dV_{ci}/d\tau$ is different: the electrons are accelerated by the HF field in these regimes instead of being retarded. Naturally, this result manifests itself only if we pass from the ‘ r ’ to the ‘ z ’ system. Thus, the contradiction between Eqns (25) and (26) is fictitious. In addition, it is important that Eqns (26) apply only in the above-specified range of A , where \bar{V} definitely increases.

The case considered above (Figs 5 and 6a) corresponds to the situation where the averaging technique is undoubtedly applicable, because the number of electron oscillations is $n_e \gtrsim 10$ and the process is truly adiabatic. Shown in Fig. 6b are the dependences $\bar{V}(A)$ and $\eta_e(A)$ in the case where the averaging conditions are not satisfied and the correspondence

is considerably violated at sufficiently large A . Here, $n_e \approx 2.5$, and there is nothing to ‘average’; all the more surprising is the fact that a qualitative correspondence is still present. We note that the physical processes occur in this case in an obviously different way. The oscillating components of the velocity remain finite due to the nonadiabatic character of the processes instead of damping to zero. As a result, if $A > 23$ and all electrons are reflected by the field, the efficiency $\eta_e(A)$ does not remain zero but its negative value further increases.

4. Nonsynchronous interaction of a relativistic electron flow with the rotating E_{11n} field of a cylindrical resonator

The content of this section is based on Ref. [28]. As shown in Ref. [29], if a relativistic electron flow (REF), rectilinear at the inlet, interacts with a strong rotating field H_{11n} of a cylindrical resonator, then efficient generation is possible at an appropriate combination of the initial speed of electrons v_0 the phase speed of the wave in the resonator v_{ph} , and the induction of the external longitudinal magnetic field B_0 , if the amplitude of the electromagnetic field reaches sufficiently high values. The output of energy by relativistic electrons is also apparently possible in a rotating H_{11n} field, with the interaction between the electrons and the longitudinal component of the electric field E_z as an accessory factor. But the basic feature of the mechanism of the interaction between a thin REF and a rotating electromagnetic field is the absence of a phase bunching of electrons (i.e., all electrons are at a right phase); this property is naturally preserved in this case. In what follows, we present the results of an analysis of the interaction between an REF and a rotating E_{11n} field. The principal simplifications in the model are the same as in Ref. [29]: the REF is thin and rectilinear, and enters the resonator axially; the volume charge is not taken into account; and the approximation of a given E_{11n} field is used (i.e., the excitation of parasitic waves is neglected). We specify the fields of the working oscillation mode at a frequency ω in the resonator as

$$\begin{aligned} \dot{E}' &= E'_m E^0(x) \exp(j\theta) = E'_m E^0(x) \exp[j(\theta + \psi_0)], \\ \dot{B}' &= \dot{B}'_m B^0(x) \exp(j\theta) = \frac{E'_m}{c} B^0(x) \exp[j(\theta + \psi_0)], \end{aligned} \quad (31)$$

$$\theta - \omega t.$$

Next, we introduce the notation

$$E = \text{Re } E^0 \exp[j(\theta + \psi_0)], \quad B = \text{Re } B^0 \exp[j(\theta + \psi_0)].$$

The equations of motion of an electron in the given field of the resonator and in a uniform longitudinal magnetic field then acquire the form

$$\frac{d(\boldsymbol{\beta}/R)}{d\theta} = -A(\mathbf{E} + [\boldsymbol{\beta}\mathbf{B}]) - F[\beta z_0], \quad \frac{dx}{d\theta} = \beta, \quad (32)$$

where

$$\begin{aligned} \mathbf{x} &= \frac{cx'}{\omega} = xx_0 + yy_0 + zz_0 = \psi\boldsymbol{\psi}_0 + r\mathbf{r}_0 + z\mathbf{z}_0, \\ \beta &= \frac{v}{c}, \quad R = \sqrt{1 - \beta^2}, \quad A = \frac{eE'_m}{m_0\omega c}, \quad F = \frac{eB_0}{m_0\omega}. \end{aligned}$$

For a rotating E_{11n} field, the components E and B are given by ($B_z = 0$)

$$\begin{aligned} E_\psi &= -0.5 \frac{k_z}{k_r} [J_0(k_r r) + J_2(k_r r)] \sin(k_z z) \sin(\theta + \psi_0 - \psi), \\ E_r &= -0.5 \frac{k_z}{k_r} [J_0(k_r r) - J_2(k_r r)] \sin(k_z z) \cos(\theta + \psi_0 - \psi), \\ E_z &= J_1(k_r r) \cos(k_z z) \cos(\theta + \psi_0 - \psi), \\ B_\psi &= 0.5 k_r^{-1} [J_0(k_r r) - J_2(k_r r)] \cos(k_z z) \sin(\theta + \psi_0 - \psi), \\ B_r &= 0.5 k_r^{-1} [J_0(k_r r) + J_2(k_r r)] \cos(k_z z) \cos(\theta + \psi_0 - \psi). \end{aligned} \quad (33)$$

In a resonator with H_{11n} oscillations, the components E and B can be written as ($E_z = 0$)

$$\begin{aligned} E_\psi &= -0.5 [J_0(k_r r) - J_2(k_r r)] \sin(k_z z) \sin(\theta + \psi_0 - \psi), \\ E_r &= -0.5 [J_0(k_r r) + J_2(k_r r)] \sin(k_z z) \cos(\theta + \psi_0 - \psi), \\ B_\psi &= 0.5 k_z [J_0(k_r r) + J_2(k_r r)] \cos(k_z z) \sin(\theta + \psi_0 - \psi), \\ B_r &= 0.5 k_z [J_0(k_r r) - J_2(k_r r)] \cos(k_z z) \cos(\theta + \psi_0 - \psi), \\ B_z &= k_r J_1(k_r r) \sin(k_z z) \cos(\theta + \psi_0 - \psi), \end{aligned} \quad (34)$$

where

$$k_z = \frac{1}{\beta_{ph}}, \quad k_r = \beta_{ph} \sqrt{\beta_{ph}^2 - 1}, \quad \beta_{ph} = \frac{v_{ph}}{c}, \quad 0 \leq z \leq \frac{n\pi}{k_z}.$$

For a thin electron flow that has negligibly small transverse velocities of electrons at the resonator inlet and that enters the resonator axially, the initial conditions for system (32) can be specified as

$$\beta(0) = \beta_0 z_0, \quad x(0) = 0. \quad (35)$$

The total electron efficiency can be defined as

$$\eta(0) = \frac{1 - R(0)/R(\theta)}{1 - R(0)}. \quad (36)$$

To match the field in the resonator and the current that excites it, equations of motion (32) must be supplemented with the excitation equation

$$\begin{aligned} A &= A \exp(j\psi_c) \\ &= \frac{2eI_0 Q}{m_0 \omega^3 \epsilon_0 \|E^0\|^2} \frac{1 + j\varphi Q}{1 + (\varphi Q)^2} \int_0^{\theta_1} \exp(-j\theta) E^0 \beta d\theta. \end{aligned} \quad (37)$$

where

$$\|E^0\|^2 = \int_{V_p} E^0 E^{0*} dV_p,$$

V_p is the volume of the resonator, I_0 is the current of the beam, Q is the quality factor of the resonator for working-mode oscillations, $\varphi = 2(\omega - \omega_0)/\omega$ is the relative detuning of the resonator (where ω_0 is its resonance frequency), and θ_1 is the phase at which the electron leaves the resonator. Equation (37) allows dividing the problem into two stages if I_0 and Q are not given: problem (32), (35), (36) with given A and ψ_0 can be separately solved first, after which the combinations of Q , I_0 ,

and φ corresponding to the regime thus found can be determined (if necessary) by calculating the integral in Eqn (37). In what follows, we use precisely this possibility of separation. Figure 7 shows the height plot of the oscillation and absorption zones on the (F, A) plane for a rectilinear REF interacting with rotating E_{111} (a), E_{112} (b), and H_{111} (c) fields at $\beta_0 = 0.9$ and $\beta_{ph} = 1.2$. The contours are labeled with the efficiency values (positive and negative); the plus signs mark the oscillation zones and the minus signs mark the absorption zones.

Comparing the structure of the oscillation and absorption zones in the above three cases yields the following inferences. The oscillation zone is the widest and least critical if the REF interacts with the E_{111} field. For the E_{112} field, the main zone is narrower and the maximum efficiency is lower; at the same time, a second oscillation zone emerges in the region of increased A and $F < 0$. The oscillation zone for the H_{111} field proves to be highly critical at high efficiencies; moreover, high efficiencies are achieved at A values twice as large as for the E_{111} fields.

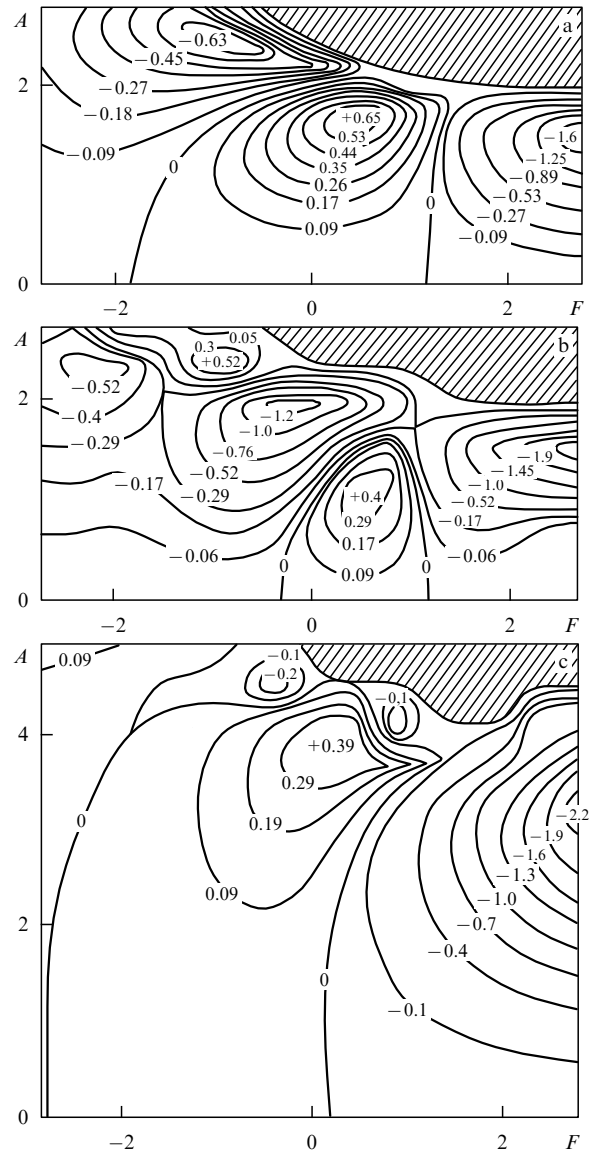


Figure 7. Height plots of the electron efficiency η on the (A, F) plane.

We also note that the generation zone at $F > 0$ in the case of the H_{111} field is separated from the region of small A by an absorption zone (the same also refers to the second zone of the E_{112} -field oscillation). This property (noted in Ref. [29]) results in a threshold effect: oscillation is possible only at finite (and sufficiently large) amplitudes of the high-frequency field. In the case of E_{111} oscillations, no threshold effect is present, which is very important for the realization of an REF-based generator. The displacement of the center of the oscillation zone in the (A, F, β_{ph}) space at $\beta_0 = 0.9$ for the E_{111} field is illustrated in Fig. 8a, where the A^0 dependences of F^0 , η^0 , and β_{ph} are shown. At small β_{ph} ($\beta_{ph} = 1.05; 1.1$), the center of the zone is located in the region of $F = 0$ (we recall that generation at $\beta_{ph} = 1$, i.e., in the T_{00n} field, is possible only if $F < 0$ [21]). As β_{ph} increases, the center of the zone shifts toward positive F (the generation zone drifts to the right in the (F, A) plane). At first, A^0 and η^0 increase (the maximum of η^0 is located in the region $\beta_{ph} \simeq 1.2$), after which η^0 decreases slowly. The β_0 dependences of A^0 , F^0 , and η^0 at $\beta_{ph} = 1.2$ are presented in Fig. 8b. They indicate that F^0 , A^0 , and η^0 increase monotonically with β_0 ; at $\beta_0 = 0.95$, the efficiency reaches 75%. At $\beta_0 > 0.9$, however, the increase in A^0 accelerates dramatically, which is obviously an undesirable effect because it both increases the losses in the resonator and restricts the generation frequency (because of reaching the breakdown strengths of the HF field). Since the interaction of the REF with the E_{111} field is most interesting, we consider precisely this case. As investigations show, the interaction mechanism remains the same throughout the entire generation zone. We therefore discuss its basic regularities using the particular example of $\beta_{ph} = 1.2$, $\beta_0 = 0.9$, $A = 1.35$, and $F = 0.445$ (this point is located below the center of the zone at the A axis, $A^0 = 1.74$). In Fig. 9a, the dependences $\beta_z(z)$, $\beta_t(z)$, and $R(z)$ are shown together with the relative value of $E_z(z)$ at the trajectory of the electron; the arrows at the z axis mark the times needed for comparisons with Fig. 9b, where the same times are marked with dots and are numbered. Figure 9b shows the trajectory of the electron in the rest frame. The interaction of the REF with a rotating E_{111} field can be divided into several stages.

(1) In the interval $0 \leq z \leq 1.5$, the action of the B_t field results in a transformation of β_z and β_t . In addition, in the end region of this section ($1 \leq z \leq 1.5$), there is a specific balance

between the accelerating action of E_z ($E_z < 0$) and the decelerating action of the component of E_t tangential to the trajectory (cf. Figs 9a and 9b, the node point 3). As a result, $R = \text{const}$ in this region.

(2) In the interval $1.5 \leq z \leq 2$ (the center of the resonator), the removal of transverse energy starts exceeding the increase in longitudinal energy, with a slow increase in R .

(3) In the interval $2 \leq z \leq 3.7$, the bulk removal of energy from the REF occurs. This is a very specific process: the electron moves in a rapidly increasing decelerating field E_z , while its longitudinal velocity increases in the interval $2 \leq z \leq 3.25$. This results from the excessive increase in β_z due to the transformation of β_t into the B_t field (for the orientation of B_t , see points 4–7 in Fig. 9b) over the decrease in β_z due to the decelerating action of the E_z field. Thus, in the interaction of the REF with the E_{111} field, the function β_t is a specific reservoir of energy for the afflux to β_z , while the direct interaction with E_t (Fig. 9b) is not significant (because the tangential component E_t is small) and plays an auxiliary role, in contrast to the interaction of the REF with the H_{111} field. The transverse component of the electron velocity, β_t , also plays another role, leading to a transverse deflection of the electron and phasing it in the field E_z [we recall that $E_z = 0$ at the axis, see Eqn (33)].

In the end region of the selection interval $3.5 \leq z \leq 3.77$, the backward turn of the beam also occurs in B_t (see point 8 in Figs 9a and 9b). Again, β_t increases there, while β_z decreases due to both braking in the E_z field and transformation into β_t . We note that this effect is not a manifestation of a ‘saturated’ or ‘oversaturated’ regime. It can also be observed at A even smaller than its optimum value. Apparently, this regime is energetically more favorable because of the delay of the electron at the braking phase of E_z , where the trajectory is reversed.

Of interest are the dependences of A^2/η on A , which characterize the starting current and the stability of the steady oscillation regime ($A^2/\eta|_{A=0}$ is proportional to the starting current I_{start} ; at a given finite A , this quantity is proportional to the working current, or to the quality factor of the resonator). Figure 10 presents dependences of A^2/η on A at $\beta_0 = 0.9$. It can be seen that no threshold effect is present in the interaction of the REF with rotating E_{111} fields, in contrast to the case of H_{111} fields [29]; this was noted above

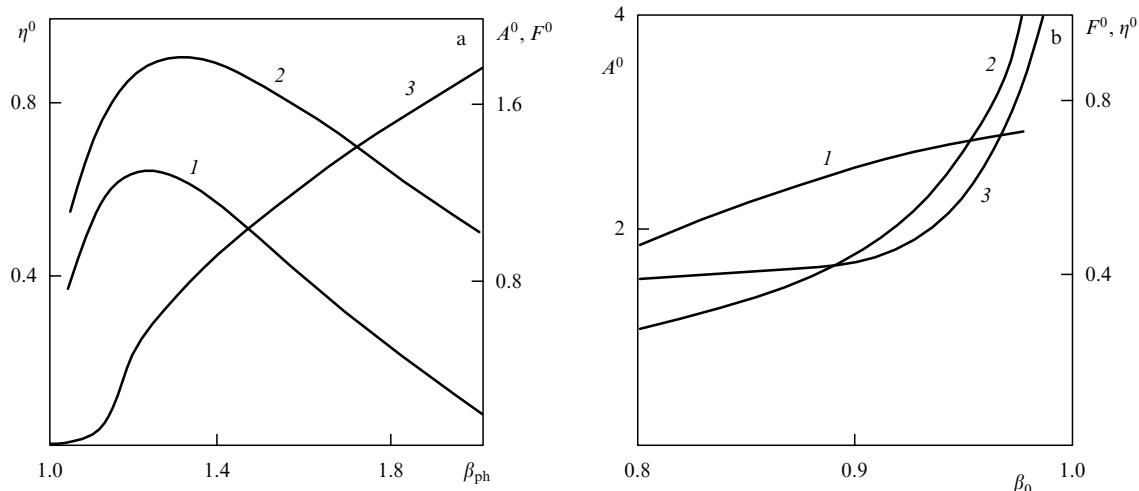


Figure 8. Dependences of the parameters η^0 (1), A^0 (2), and F^0 (3), optimal in terms of efficiency, on β_{ph} (a) and β_0 (b).

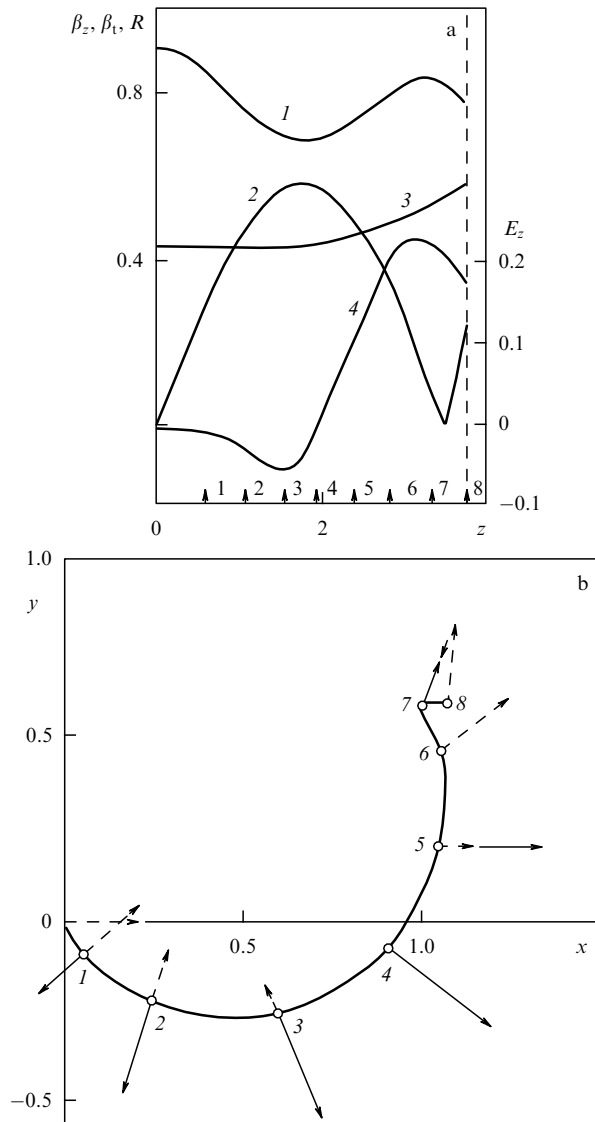


Figure 9. (a) Characteristics of electron motion along the trajectory: 1, β_z ; 2, β_t ; 3 R ; 4, E_z ; (b) the transverse trajectory of the electron: solid arrows, the direction of E_t ; dashed arrows, the direction of B_t .

based on our analysis of the structure of the oscillation zones. In principle, a hard excitation regime is possible for $0.4 \leq A \leq 1.3$ (curves 1 and 2); in this case, the working current is smaller than the starting current. However, in high-efficiency regimes (curve 2) at $A = 1.74$, the working current exceeds the starting current, and the slope of the A dependence of A^2/η is positive, which testifies to the stability of the steady oscillation regime. Curves 3–5 reflect the fact that the slope of the A^2/η curve is everywhere positive, i.e., that the steady oscillation regime is stable at any quality factor.

Thus, our investigation of the interaction of a rectilinear REF with rotating E_{111} fields reveals three basic advantages of this type of interaction in the oscillator compared with the case of H_{11n} fields [29]: (1) no threshold effects are present; (2) the working strength is reduced by half; and (3) the oscillation zones are not critical at high efficiencies. At the same time, the following feature should be noted: removers with E_{111} -type oscillations in amplifiers with pre-swept REFs can ensure efficiencies approaching unity, in contrast to removers with H_{111} -type oscillations. If we also take into account that the

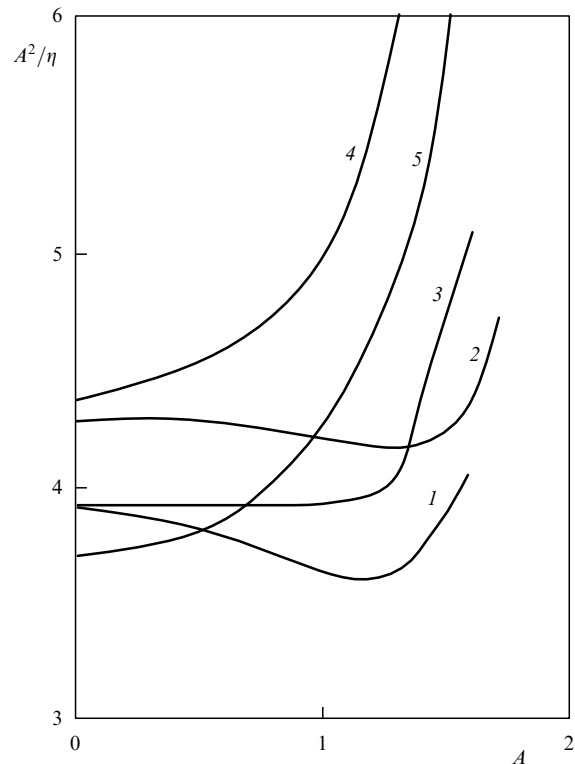


Figure 10. Dependences of A^2/η on A at various conditions of interaction: 1 — $\beta_{ph} = 1.1, F = 0$; 2 — $\beta_{ph} = 1.2, F = 0.44$; 3 — $\beta_{ph} = 1.2, F = 0$; 4 — $\beta_{pg} = 1.2, F = 0.4$; 5 — $\beta_{ph} = 1.5, F = 0.8$.

removers with E_{111} -type oscillations can exhibit self-excitation (without a pre-sweep of the REF), while the removers with H_{111} -type oscillations cannot (because of the threshold phenomena), it becomes clear that the E_{111} type oscillation can be recommended for generators and the H_{111} type for removers in amplifiers.

5. Coaxial oscillator with a nonsynchronous interaction

The content of this section is based on the material in Ref. [30]. Currently, medium-power microwave oscillators are needed for many purposes; their basic advantages are small weights and sizes (e.g., due to the absence of magnetic focusing systems), as well as simple and highly reliable arrangements. Their efficiency is not a primary factor. The field of application of such oscillators is very wide: portable, durable medical and technological setups, devices for training laboratories and measuring antenna equipment, etc. These needs dictated the search for oscillation mechanisms complying with these requirements. As frequently happens, this search led to the well-known diode and monotron arrangements [31–34]. However, their efficiency is unacceptably low, $\approx 6\%$. Therefore, we here consider an inverted cylindrical-diode (and monotron) arrangement with a coaxial resonator. In such arrangements, electrons move in the direction of an increasing HF field; it is known that although bunching faults are inherent in nonsynchronous interaction, such a pattern of motion can be expected to substantially increase the efficiency. As shown in this section, the electron efficiency of a monotron (with the volume charge taken into account) can in principle reach 33% and that of a diode, 24%.

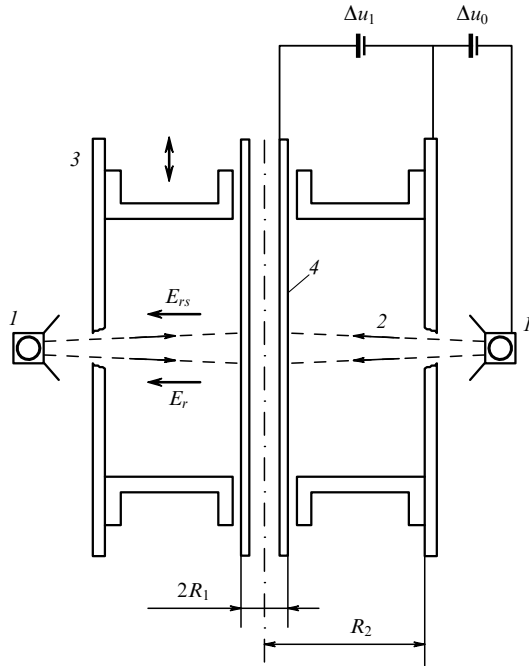


Figure 11. The arrangement of a diode oscillator, diotrone.

Figure 11 shows an oscillator arrangement that we consider in the case of a monotron. The electron gun, 1, forms a planar disk-shaped electron flow, 2, which passes through the coaxial resonator, 3, in the region of the maximum electric component of the lowest eigenmode T_1 and interacts with the latter. The voltage Δu_0 determines the initial speed of the electrons entering the interaction region, and Δu_1 is the accelerating voltage in the interaction region. If electrons are emitted from the resonator wall at zero speed, the arrangement becomes simpler, with $\Delta u_0 = 0$ (which corresponds to a diode). The waste electrons settle to the inner cylinder, which plays the role of the anode (in contrast to the experiments in Ref. [31], where the inner cylinder was the cathode). The electrons in the flow move through the interaction region (Fig. 11) under the action of a constant electric field E_r and a variable electric field E_{rs} :

$$E_r = \frac{\Delta u_1}{\ln(R_2/R_1)} \frac{1}{r}, \quad E_{rs} = \frac{\Delta u_s}{\ln(R_2/R_1)} \frac{1}{r} \cos(\omega t + \varphi). \quad (38)$$

Here, R_1 and R_2 are the radii of the inner and outer cylinders of the coaxial resonator, r is the distance from the resonator axis, $R_1 \leq r \leq R_2$, Δu_1 is the potential difference between the cylinders, Δu_s is the amplitude of the HF oscillations of the electromagnetic field excited in the resonator, ω is the working frequency of the oscillation, and φ is the initial phase. According to large-particle method, we represent the electron flow as an ensemble of N ring particles, which are initially uniformly distributed over the oscillation period. The field of the volume charge acting on the i th particle and produced by other particles can then be approximately written as

$$E_{qi} = \frac{I_0}{\omega r_i 2\pi \epsilon_0} \frac{1}{N} \sum_{\substack{j=1 \\ j \neq i}}^N \frac{1}{r_i - r_j}, \quad (39)$$

where I_0 is the beam current, ϵ_0 is the vacuum dielectric constant, and r_i and r_j are the radii of the ring particles.

We introduce the variable $z = R_2 - r$, measured in the direction of particle motion, and write the dimensional equations of motion of large particles in the 'z' coordinate system as

$$\frac{dv_i}{dz} = \frac{e(E_r + E_s + E_{qi})}{m_0 \gamma_i^3 v_i}, \quad \frac{dt_i}{dz} = \frac{1}{v_i}, \quad (40)$$

where v_i is the velocity of the i th particle, t_i is the individual time, e and m_0 are the charge and mass of the electron, $\gamma_i = 1/\sqrt{1 - v_i^2/c^2}$, and c is the speed of light.

For convenience, we pass to dimensionless variables, viz., $V_i = v_i/v_0$, where v_0 is a reference value of the electron speed,

$$\beta_0 = \frac{v_0}{c}, \quad \gamma_0 = \frac{1}{\sqrt{1 - \beta_0^2}}, \quad \gamma_i(T) = \frac{1}{\sqrt{1 - V_i^2(T) \beta_0^2}},$$

$$L = R_2 - R_1, \quad \delta = \frac{R_1}{L}, \quad T = \frac{z}{L}, \quad u_i = \omega t_i - \frac{z\omega}{v_0},$$

$$\theta_0 = \frac{\omega L}{v_0}, \quad A = \frac{e\Delta u_1}{m_0 v_0^2}, \quad A_s = \frac{e\Delta u_s}{m_0 v_0^2},$$

$$D_1 = \ln \frac{\delta + 1}{\delta}, \quad S_q = \frac{eD_1 I_0}{m_0 2\pi \epsilon_0 v_0^3}, \quad F_{qi} = \frac{1}{N} \sum_{j=1}^N \frac{1}{u_i - u_j}.$$

In passing from Eqn (39) to F_{qi} , we use a linear extrapolation of u_j , as is usually done for O-type devices. In these variables, Eqns (40) is written as

$$\frac{dV_i}{dT} = \frac{A + A_s \cos(u_i + \theta_0 T) + S_q F_{qi}}{V_i \gamma_i^3 D_1 (\delta + 1 - T)}, \quad (41)$$

$$\frac{du_i}{dT} = \theta_0 \left(\frac{1}{V_i} - 1 \right).$$

For a monotron, the reference velocity v_0 is chosen to be equal to the entry velocity of the electrons at the resonator inlet; it can be calculated from the accelerating voltage Δu_0 in accordance with the relation $e\Delta u_0 = mc^2(\gamma_0 - 1)$. Without the relativistic corrections,

$$v_0^2 \cong \frac{2\Delta u_0 e}{m_0}, \quad A \cong \frac{1}{2} \frac{\Delta u_1}{\Delta u_0}, \quad A_s \cong \frac{1}{2} \frac{\Delta u_s}{\Delta u_0}.$$

For a diode, the electrons have zero initial velocity ($\Delta u_0 = 0$), and the reference velocity v_0 is calculated from the accelerating voltage Δu_1 using the relation $e\Delta u_1 = mc^2(\gamma_0 - 1)$. If the relativistic correction is ignored,

$$v_0^2 = \frac{2\Delta u_1 e}{m_0},$$

with $A \cong 0.5 = \text{const}$ and $A_s \cong 0.5\Delta u_s/\Delta u_1$.

The initial conditions at $T = 0$ are

$$u_i = (i - 0.5) \frac{2\pi}{N}, \quad i = 1, \dots, N, \quad (42)$$

where $V_i = 1$ for the monotron and $V_i = 0$ for the diode.

The efficiency of the interaction can be estimated based on the electron efficiency, which is the ratio of the difference between the mean electron energies before and after the interaction with the HF field to the electron energy corresponding to the potential difference $\Delta u_0 + \Delta u_1$:

$$\eta_e(T) = \frac{1}{N} \sum_{i=1}^N \frac{\gamma_0 - \gamma_i(T) + A\beta_0^2 \ln((\delta + 1)/(\delta + 1 - T))/D_1}{\gamma_0 - 1 + A\beta_0^2} \quad (43)$$

for the monotron and

$$\eta_e(T) = \frac{1}{N} \sum_{i=1}^N \left[\frac{\ln((\delta + 1)/(\delta + 1 - T))}{D_1} - \frac{\gamma_i(T) - 1}{\gamma_0 - 1} \right]$$

for the diode. The degree of particle bunching can be estimated using the bunching function

$$G_r = \sqrt{\left(\frac{1}{N} \sum_i \cos u_i\right)^2 + \left(\frac{1}{N} \sum_i \sin u_i\right)^2} \quad (44)$$

If no bunching is present, $G_r = 0$; if the bunching is perfect, $G_r = 1$.

The interaction process in the considered oscillator is determined by four basic dimensionless parameters: the relative value A of the accelerating voltage in the interaction region, the relative amplitude A_s of the HF field, the transit angle, θ_0 , and the geometrical factor of the resonator δ . Two additional parameters, β_0 and A_q , describe the relativistic effects (if $\beta_0 > 0.3$) and the role of the interaction of electrons at high beam currents, respectively.

Two radically different regimes can be realized in the arrangement under discussion. The first is the diode regime in which electrons are emitted directly from the wall of the outer cylinder of the resonator (the cathode of the gun, l , coincides with the wall; $\Delta u_0 = 0$). The second is the monotron regime in which the electrons of the flow produced by the gun enter the resonator at the initial speed v_0 determined by the potential difference Δu_0 and interact with the HF field. An additional accelerating voltage Δu_1 is in this case necessary for the electrons settling into the inner cylinder. In both cases, solutions of problem (41), (42) were obtained and specific features of the regimes revealed.

The diode regime. In this case, the arrangement of the generator is especially simple. In the calculations, which took into account that $V_i = 0$ at $T = 0$, Eqns (41) were written in the ‘ r ’ system, and the field of the bulk charge was neglected ($S_q = 0$). Thus, the problem was described by three parameters: A_s , θ_0 , and δ . Figure 12a presents a dependence $\eta(T)$ typical of three cases with different transit angles θ_0 . At large transit angles θ_0 , the quantity $\eta(T)$ changes its sign periodically with an increase in T . The regions of positive η correspond to the removal of the kinetic energy of the electrons by the electromagnetic wave. The oscillation amplitude of $\eta(T)$ increases with T because of the increase in the HF-field amplitude. Generation occurs if $\eta(1) > 0$ at the end of the interaction region. If A_s and δ are fixed, generation can be successively observed with increasing θ_0 at the first, second, and consequent maxima (zones). The

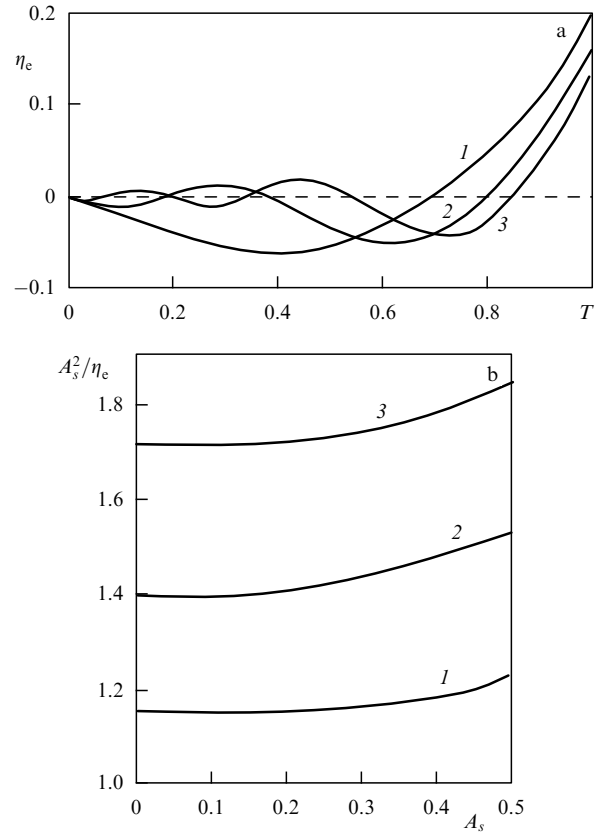


Figure 12. The characteristics of a diode at $A_s = 0.5$ and $\delta = 0.1$ in three cases: 1, $\theta_0 = 2.21$, $\eta(1) = 0.205$; 2, $\theta_0 = 4.47$, $\eta(1) = 0.162$; 3, $\theta_0 = 6.68$, $\eta(1) = 0.135$. (a) The T dependences of the electron efficiency; (b) the A_s dependences of A_s^2/η_e .

generation mechanism operates because the electrons of the flow, at the very beginning of their motion, experience velocity modulation in the field of the HF wave, which has a finite amplitude, $A_s/(1 + \delta)$, at $T = 0$. As a result, the subsequently formed bunch passes alternately through decelerating and accelerating phases of the HF field, whose amplitude increases. The energy exchange is most intense near the inner electrode, where the amplitude of the HF field increases sharply if δ is small. The parameters should be chosen so as to position the positive maximum at the end of the region ($T = 1$). Calculations show that the location of the maximum $\eta(1)$ is independent of A_s and is determined by the parameters θ_0 and δ . As A_s increases, the quantity $\eta(1)$ decreases monotonically. For $A_s > 0.5$ ($\Delta u_s > \Delta u_1$), a fraction of the electrons is locked by the HF field at the cathode; we therefore carried out our computations for $A_s \leq 0.5$. Figure 12 shows various cases for a fixed $\delta = 0.1$ at which the amplitude of the field increases over the extent of the interaction region by approximately a factor of 10. The θ_0 values are chosen such that $\eta(1)$ corresponds to a maximum. As δ decreases, $\eta(1)$ increases and the θ_0 value corresponding to the maximum decreases.

It can be seen from the Table (where the superscripts correspond to the numbers of the working maxima) that the efficiency of the oscillator can reach 24% in the first zone, which substantially exceeds the efficiency of the plane diode generator ($\cong 6\%$ [31]). As the zone number is increased by unity, the quantity $\eta(1)$ decreases by a factor of about 1.2. Given the values of the loaded quality factors Q , δ , and Δu_1 ,

Table. Diode parameters at $A_s = 0.5$.

δ	θ_0^1	$\eta^1(1)$	θ_0^2	$\eta^2(1)$	θ_0^3	$\eta^3(1)$
1.0	3.20	0.13	6.14	0.08	8.97	0.06
0.1	2.21	0.20	4.47	0.16	6.68	0.13
0.05	2.06	0.22	4.02	0.18	6.04	0.16
0.025	1.82	0.24	3.69	0.22	5.59	0.18

we can compute the working current of the generator as

$$I_0 = \frac{\pi \varepsilon_0 c \Delta u_1}{\ln[(\delta + 1)/\delta] Q} \frac{A_s^2}{\eta(1)}. \quad (45)$$

As $A_s \rightarrow 0$, formula (45) determines the starting current I_{start} . Figure 12b presents the A_s dependences of A_s^2/η_e , which indicate that $I_{\text{start}} < I_0$, i.e., the excitation regime of the diotron is soft.

The monotron regime. This form of the generator allows varying the parameter A , the ratio of the constant accelerating voltages. At $A = 0$, there is no accelerating voltage inside the interaction region. In this case, the electrons of the flow move inertially to the inner cylinder in the HF field of increasing amplitude. Because of the initial and dynamical spread in the velocities of electrons in the flow, a portion of the electrons can be reflected from the inner cylinder, which is undesirable. To avoid this effect, an additional accelerating voltage Δu_1 is created, which ensures the settling of all electrons in the flow to the inner cylinder. At $A = 0.5$, the relation $\Delta u_1 \cong \Delta u_0$ holds, and therefore all electrons settle to the anode. Problem (41), (42) was solved taking the field of the volume charge at voltages $\Delta u_0 + \Delta u_1 \leq 5$ kV into account; therefore, relativistic effects were insignificant, and the results could be used at $\beta_0 \leq 0.15$. Calculations have shown that the actual transit angle decreases with increasing A without changes in the character of the interaction. As A_s increases to a certain value depending on δ and θ_0 , the quantity $\eta(1)$ increases monotonically (after this value has been exceeded, electrons decelerated to zero velocity emerge). In contrast to the diode arrangement, $\eta(1)$ reaches its maximum at a certain relation between the parameters A_s , δ_0 , and θ_0 ; they can be found from the condition for the maximum of $\eta(1)$.

For this regime, Fig. 13a presents typical T dependences of the interaction parameters at the optimum values of A_s , δ_0 , and θ_0 , which correspond to the generation regimes at the first, second, and third maxima (zones). The $\eta(T)$ dependences are similar to the above-described diode characteristics. It can be seen from the behavior of the $G_r(T)$ curves that the electrons of the flow, after acquiring their initial velocity modulation, are gathered into fairly compact bunches (with G_r reaching 0.65), and G_r increases only where η decreases, i.e., as the bunch passes through the accelerating phase of the field. The decelerating-phase center at the entry to the interaction region corresponds to the center of the bunch. The bunching process is illustrated in Fig. 13b, where the phase trajectories of electrons are given in the form of $T_i(\omega t)$ dependences, i.e., in the ‘ t ’ system. A compact bunch passing through the end section of its path through high-amplitude fields of a decelerating phase releases a larger portion of its kinetic energy, the larger the field amplitude at this section and the higher the bunching level.

In the arrangement under consideration, the profile of the field amplitude is determined by a single parameter, δ , whose optimum value decreases with an increase in the number of the working maximum. With increases in the number of the

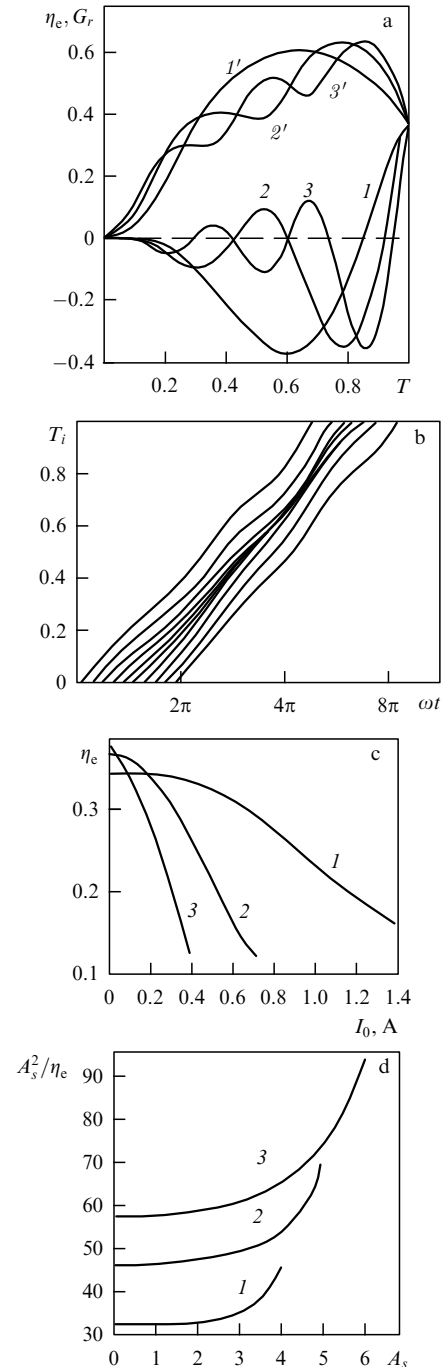


Figure 13. Characteristics of the monotron generator arrangement at $A = 0.5$ in three cases: 1, $\theta_0 = 8.18$, $A_s = 3.96$, $\delta = 0.41$; 2, $\theta_0 = 15.31$, $A_s = 5.12$, $\delta = 0.18$; 3, $\theta_0 = 22.2$, $A_s = 6.00$, $\delta = 0.1$. (a) The T dependences of the electron efficiency (1, 2, 3) and of the function G_r (1', 2', 3'); (b) the trajectories of electrons in case 2; (c) the dependences of the electron efficiency on the working current I_0 ; (d) the A_s dependences of A_s^2/η_e .

working zone, the efficiency becomes somewhat higher due to the achievement of higher bunching levels and the shortening of the selection-interval length. Calculations have shown that the efficiency in the considered arrangement reaches 37% (in a plane-parallel monotron, 19%). It can be conjectured that the efficiency of the interaction can be increased by a factor of 1.5–2 by choosing a similar profile of the HF-field amplitude and the accelerating voltage in a different arrangement, which could ensure optimum conditions of the initial modulation,

subsequent bunching, and energy removal. Presented in Fig. 13c are computational results with the volume-charge field taken into account. It can be seen that as the working current I_0 increases, the repulsion forces prevent bunching, and hence the efficiency decreases. The criticality to the growth of the current increases dramatically with the number of the working zone.

For the monotron, the working current can be calculated as

$$I_0 = \frac{\pi \varepsilon_0 c \Delta u_0}{(1 + 2A) \ln[(\delta + 1)/\delta]} \frac{A_s^2}{Q \eta(1)}. \quad (46)$$

In the limit $A_s \rightarrow 0$, the current $I_0 \rightarrow I_{\text{start}}$. Soft excitation is an important property of the monotron regime. It can be seen from Fig. 13d, where typical A_s dependences of A_s^2/η_c are presented for the first three generation zones, that the starting current is much smaller than the working current. As the number of the working maximum increases at a fixed quality factor of the resonator, the starting current increases. Of considerable importance is the issue of the wavelength ranges in which the diotron parameters are realizable. For this reason, we present here, for illustration, the following cases corresponding to θ_0 and δ from Fig. 13 at $L = 1$ cm, $\Delta u_0 = \Delta u_1 = 1$ kV, and $I_0 = 0.2$ A. For the first zone, $\lambda = 11.5$ cm and $Q = 841$; for the second, $\lambda = 6.32$ cm and $Q = 928$; and for the third, $\lambda = 4.35$ cm and $Q = 1252$. At the same time, the quality factor Q_c of the copper coaxial resonator itself exceeds 12,000 in the above wavelength ranges. Therefore, the circuit efficiency $\eta_k = 1 - Q/Q_c$ is in excess of 90% in all ranges.

6. The effect of nonsynchronous azimuthal spatial harmonics on the peniotron efficiency

The content of this section is based of the material in Ref. [35]. The peniotron was invented in the early 1960s [36]. It is among the few microwave devices in which a virtually perfect, in terms of efficiency, interaction mechanism is realized: all electrons of a thin-wall tubular beam, which rotates in a longitudinal magnetic field B_0 coaxially with an azimuthally periodic electrodynamic system, give the same average energy up to the HF field, irrespective of their initial relative phase in the T field ($v_{\text{ph}} = c$). This occurs if the following peniotron-synchronism condition is satisfied:

$$1 - \frac{v_z}{v_{\text{ph}}} = p\Omega, \quad p = n - 1, \quad \Omega = \frac{eB_0}{\gamma m_0 \omega},$$

where v_z is the longitudinal velocity of electrons, v_{ph} is the phase speed of the wave that has n azimuthal variations, and p is the number of the synchronous harmonic. In this case, as simplified analytical models indicate [37], the efficiency of the peniotron interaction remains high with the increase in the number of the synchronous harmonic to $p = 10$. This raised hopes of developing an efficient, medium-power, millimeter-wave source ($P_{\text{out}} \approx 1-10$ kW) with permanent magnets, based on this mechanism, which could ensure the required level of B_0 .

The inadequacy of the one-electron model under certain conditions was first noted in [38]. In calculations based on a nonaveraged model, the author revealed a substantial dependence of the efficiency on the initial phase of electrons at $v_{\text{ph}} > c$ and in the relativistic case. Nonaveraged models of

the peniotron amplifier and oscillator using a T wave in a multiply connected electrodynamic system were proposed in Ref. [39]. Such a system is best for the efficient realization of the peniotron mechanism because not only the condition $v_{\text{ph}} = c$ is satisfied there but also the electron orbits of the weakly relativistic beam can be brought nearer to the lamellas of the electrodynamic structure in the intense-field region.

The investigations of the optimum arrangements based on such models with the effect of the volume-charge field taken into account indicate that the efficiency of the peniotron amplifier becomes considerably lower due to the action of the volume-charge field, which results in a dependence of the interaction energies on the entry phase of the electron, especially at larger numbers of the synchronous harmonics. As the calculations in Refs [40–42] show, the efficiency of the peniotron generator at optimally chosen parameters remains fairly high (reaching 72% at $p = 3$ and 34% at $p = 10$), although the backward partial wave has a negative effect if there are conditions close to those of the gyroresonant wave–beam interaction.

An analysis of the optimum arrangements of the peniotron oscillator has shown that the action of the volume-charge-field forces can be compensated because conditions are created under which the amplitude of the HF field far exceeds these forces. In practice, this is possible if the quality factor of the resonator and the power of the beam are properly balanced. According to experimental data [43], a proper choice of the loaded quality, $Q \approx 2000$ for $p = 3$, can ensure the required amplitude of the HF field and allow obtaining an efficiency of 70%, in agreement with calculations. At $p = 10$, the calculated efficiency is 33%, while only a 6% efficiency was achieved in experiment. As calculations show, the optimum efficiency can be obtained if the quality factor of the resonator is five times as large as realized experimentally. A similar experimental result was reported in Ref. [44].

A drawback of the available mathematical models is that the field of the electrodynamic system is represented by only one synchronous harmonic with an azimuthal dependence of the form $\exp(-jm\psi)$. For this approximation, the ‘perfection’ of the peniotron interaction mechanism was noted in the nonrelativistic case. However, an HF field is actually not azimuthally harmonic, i.e., it includes nonsynchronous components with distributions of the form $\exp(-jkm\psi)$. Obviously, these components destroy the ‘perfection’ of the peniotron mechanism, and their effect must be taken into account in considering a peniotron.

We have carried out such computations for a centimeter-wave peniotron generator with a resonator in the form of a segment of a multiply connected waveguide in which the π type of the T_{21l} mode is realized [39] (the phase shift between neighboring lamellas is π). The vector potential for the T_{21} wave was calculated using a mesh technique virtually exactly, which allowed finding the electron interaction pattern near the lamellas, where the distribution of the HF field differs from that represented by one synchronous harmonic, as in Ref. [39]. It has been found that the presence of nonsynchronous harmonics results in a dependence of the interaction on the initial entry phase of the electrons and, accordingly, in a decrease in the efficiency. It has been shown that using ellipsoidal lamellas allows substantially reducing the level of nonsynchronous harmonics and enhancing the efficiency of the peniotron.

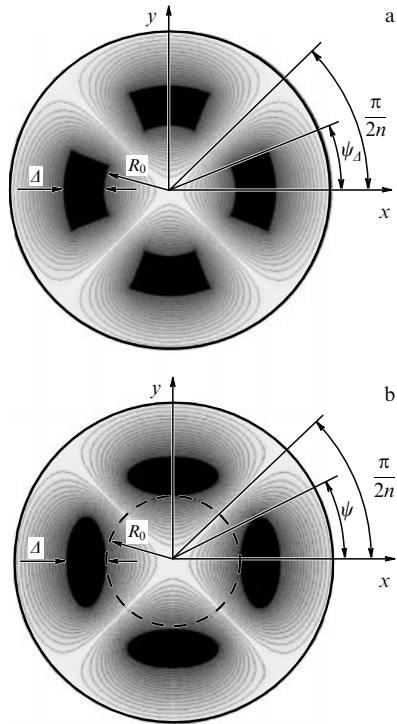


Figure 14. The cross section of the interaction region in the peniotron.

The geometry of the cross section of the interaction region for two different lamella profiles is shown in Figs 14a and 14b. The tubular beam rotating about its axis in a longitudinal magnetic field B_0 interacts in the working region with the T_{21l} mode excited in the resonator (π mode). We use the notation and the dimensionless mathematical model described in Ref. [39], with the effect of the volume-charge field taken into account. To include the effect of nonsynchronous harmonics, we compute the components of the HF field as follows. We represent the dimensionless components of the T_{21l} -mode electromagnetic field in terms of the V_l component of the vector potential,

$$\{E_r, E_\psi, B_r, B_\psi\} = \text{Re} \{ \dot{E}_r, \dot{E}_\psi, \dot{B}_r, \dot{B}_\psi \} \exp(jW\theta),$$

$$\dot{E}_r = W \frac{\partial V_l}{\partial r}, \quad \dot{E}_\psi = W \frac{1}{r} \frac{\partial V_l}{\partial \psi}, \quad \dot{B}_r = -j \frac{1}{r} \frac{\partial^2 V_l}{\partial z \partial \psi},$$

$$\dot{B}_\psi = j \frac{\partial^2 V_l}{\partial z \partial r}, \quad V_l = V(r, \psi) \sin z, \quad W = \frac{\omega}{\omega_0}.$$

The function $V(r, \psi)$ satisfies the Laplace equation

$$r \frac{\partial}{\partial r} \left(r \frac{\partial V}{\partial r} \right) + \frac{\partial^2 V}{\partial \psi^2} = 0. \quad (47)$$

In view of the azimuthal symmetry, the solution of Eqn (47) for the T_{n1} mode can be sought in the sector $0 \leq \psi \leq \pi/2n$, $0 \leq r \leq R$ (Fig. 14).

Values of the function V at contiguous lamellas were specified to be unity, ± 1 . At the boundaries of the computation sector,

$$\begin{aligned} \text{at } r = R \text{ and } r = 0, \quad & V = 0, \\ \text{at } \psi = 0, \quad & \frac{\partial V}{\partial \psi} = 0 \text{ (symmetry condition)}, \\ \text{at } \psi = \frac{\pi}{2n}, \quad & V = 0. \end{aligned} \quad (48)$$

Problem (47), (48) was solved using a finite-element technique in the MATLAB system. After that, the amplitude of the HF field A and the associated magnetic field B_0 were obtained based on the model described in Ref. [39] via efficiency optimization. A specific property of a medium-power peniotron oscillator is that the length of the interaction region at the beam voltages $U_0 = 1-20$ kV is $L' = (0.5-1.5)\lambda$ ($L = \pi - 3\pi$), in contrast to millimeter-wave peniotrons, where this length is normally $(10-15)\lambda$.

We analyze the computer-simulated arrangements of oscillators in which output powers 4–15 kW are ensured with efficiencies of 70–85% for the frequency $f = 915$ MHz ($\lambda = 32.7$ cm), which is used in technological setups, at the voltage $U_0 \approx 10$ kV and the beam current $I_0 \approx 0.5-2$ A. In the chosen variables, the loaded quality of the T_{n1l} -mode resonator can be calculated as

$$Q = \frac{\omega E}{\eta I_0 U_0} = \frac{\varepsilon_0 c^3 A^2 m_0 \pi W}{4e_0 I_0 (\gamma_0 - 1) \eta} \times \iint_S \left[\left(\frac{\partial V}{\partial r} \right)^2 + \left(\frac{1}{r} \frac{\partial V}{\partial \psi} \right)^2 \right] r dr d\psi,$$

where η is the electron efficiency, ω is the working frequency, E is the stored resonator energy, and S is the cross section of the interaction region.

In the computations in Refs [40,42], the HF field involved only one synchronous harmonic, i.e., it was assumed that $\dot{V} = r^n \sin z \exp(-jm\psi)$ in the interaction region. Therefore, near the lamellas, i.e., at r close to R_0 , this approximation substantially diverges from the reality. Figure 15 presents the dependence

$$E_\psi = \frac{1}{r} \frac{\partial V(r, \psi)}{\partial \psi}$$

for a resonator with rectangular lamellas at varying $r \leq R_0$ (curve 1 corresponds to $r = 0.5 R_0$, curve 2 to $r = 0.75 R_0$, and curve 3 to $r = 0.95 R_0$). It can be seen from the graph that as r approaches R_0 , the sinusoidal distribution is distorted and gradually changes into a step function. As comparative calculations show, taking the actual distribution of the field near the lamellas into account results in an additional dependence of the interaction on the initial phase of the electrons. In this case, as the synchronous radius r_0 of the electron flow approaches the lamellas, the maximum efficiency decreases. Computations of the field based on mesh techniques show that the level of spatial harmonics can be reduced if a rounded lamella is used. The dependence of the efficiency on R_0/r_0 for the one-harmonic approximation of

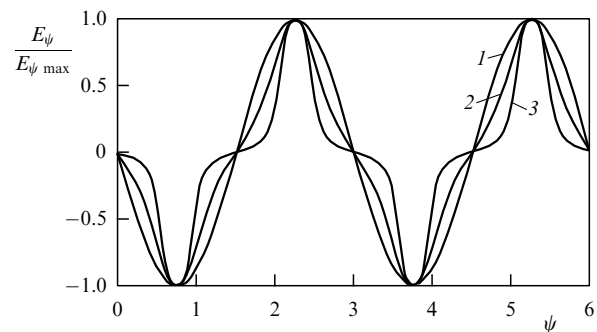


Figure 15. Change of the $E_\psi(\psi)$ dependence in approaching the lamellas.

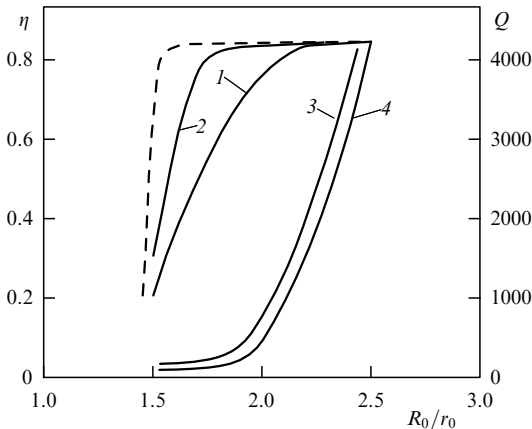


Figure 16. Dependence of η and Q on the position of the beam radius relative to the lamellas.

the field is shown with the dashed curve in Fig. 16. An abrupt decrease is observed as the trajectories of the electrons reach the radius R_0 , and electrons start settling into lamellas.

The efficiencies calculated with the inclusion of the spatial harmonics for lamellas with rectangular cross sections (curve 1) and rounded cross sections (2) coincide at large R_0/r_0 with the efficiencies based on the ideal model, because the distribution of E_ψ differs little from a sinusoidal one. As R_0/r_0 is reduced from 2 to 1.5, curve 1 declines sharply. That is because the electrons, due to the drift of the guiding centers, approach the lamellas and find their way into the field with intense spatial harmonics. The efficiency curve for a resonator with rounded lamellas begins declining at smaller R_0/r_0 , because the amplitude of the spatial harmonics is much smaller in this case. Curves 3 and 4 represent the required values of the quality factor Q for the respective arrangements with rounded and rectangular lamellas. Apparently, the quality factor necessary for a resonator with rounded lamellas is higher than for a resonator with rectangular lamellas; but in the region of working values $Q < 1000$, this enhancement is not significant compared to the gain in efficiency.

The dependences presented here were obtained for the following parameters of the beam: $\beta_0 = 0.2$, $q = 2$, $r_0 = 0.196$, $\Delta = 0.083$, $\psi_\Delta = 22^\circ$, $R_0/R = 0.6$, $\lambda = 32.7$ cm, $U_0 = 10.5$ kV, $I_0 = 1$ A, $L' = \lambda$, and $B_0 = 0.0304$ T. The lamella radius R_0 varied from 0.295 to 0.491; the amplitude A_0 and the accompanying magnetic field B_0 were optimized at each point. Energy is mainly removed from the transverse component β_t of the electron velocity near the maxima of the E components of the HF field. A slight decrease in the longitudinal component β_z is because it is transformed into the transverse component at the maximum of the magnetic component of the HF field. For a resonator with rectangular lamellas, taking the three-dimensional harmonics into account increases the spread in electron energies tenfold.

The results discussed here were obtained without the inclusion of the forces of the volume-charge field, to isolate the pure effect of the nonsynchronous components. Taking these forces into account also reduces the efficiency and increases the spread in the electron energy: the efficiency is 83% at the current 0.5 A, but it declines nearly linearly to 36% as the current is increased to 5 A.

It follows from Fig. 16 that to achieve high efficiencies (> 70%) at a realized loaded-quality factor for a resonator

with rectangular lamellas, the ratio R_0/r_0 should be chosen to be roughly 2. Using rounded lamellas allows reducing R_0/r_0 to 1.7 and bringing the electron flow closer to the region of strong fields near the lamellas, thus reducing the required loaded quality factor Q .

Below, we present optimized arrangements of the peniotron oscillator based on using the first harmonic of the cyclotron frequency at the parameters $\lambda = 32.7$ cm and $U_0 = 10.5$ kV. The first three cases correspond to a peniotron with a rectangular-lamella resonator. Cases 4 and 5 were considered for rounded lamellas. In each case, the beam current I_0 and the length of the resonator L' were fixed; the HF-field amplitude E_m and the guiding magnetic field E_m were optimized in terms of efficiency, which yielded the efficiency B_0 , the output power η , and the loaded quality factor P_{out} .

Case 1:

$$R_0/r_0 = 2 \quad I_0 = 2 \text{ A}, \quad L' = \lambda, \quad E_m = 1.35 \text{ kV cm}^{-1},$$

$$B_0 = 0.0304 \text{ T}, \quad \eta = 0.78, \quad P_{out} = 16.3 \text{ kW}, \quad Q = 400.$$

Case 2:

$$R_0/r_0 = 2, \quad I_0 = 0.5 \text{ A}, \quad L' = \lambda, \quad E_m = 1.62 \text{ kV cm}^{-1},$$

$$B_0 = 0.031 \text{ T}, \quad \eta = 0.83, \quad P_{out} = 4.3 \text{ kW}, \quad Q = 900.$$

Case 3:

$$R_0/r_0 = 2, \quad I_0 = 0.5 \text{ A}, \quad L' = 0.5\lambda, \quad E_m = 3.43 \text{ kV cm}^{-1},$$

$$B_0 = 0.030 \text{ T}, \quad \eta = 0.77, \quad P_{out} = 4.0 \text{ kW}, \quad Q = 1900.$$

Case 4:

$$R_0/r_0 = 1.7, \quad I_0 = 0.5 \text{ A}, \quad L' = \lambda, \quad E_m = 1.20 \text{ kV cm}^{-1},$$

$$B_0 = 0.030 \text{ T}, \quad \eta = 0.81, \quad P_{out} = 4.2 \text{ kW}, \quad Q = 540.$$

Case 5:

$$R_0/r_0 = 1.7, \quad I_0 = 0.5 \text{ A}, \quad L' = 0.5\lambda, \quad E_m = 2.54 \text{ kV cm}^{-1},$$

$$B_0 = 0.030 \text{ T}, \quad \eta = 0.78, \quad P_{out} = 4.1 \text{ kW}, \quad Q = 1200.$$

The first case corresponds to large values of the microperveance of the beam, which allows achieving a high output power at the electron efficiency close to 80%. In the second case, the current is reduced by a factor of four, such that the electron efficiency is increased by 6%, although the output power is reduced fourfold and the loaded quality factor increased twofold. In the fourth and fifth cases, employing rounded lamellas brought the electron beam closer to the intense-field region, reducing the quality factor without reducing the efficiency.

Our studies suggest that the nonharmonic azimuthal structure of the HF field in the peniotron plays an important role in reducing its efficiency. This structure must be taken into account in the mathematical model of the peniotron. Based on such a more complete model, the optimum parameters of the peniotron can be chosen so as to minimize the effect of nonsynchronous azimuthal harmonics. We note that, as we show below, the phase trajectories of the electrons are nearly congruent in this case, and the spread in the electron energies in the flow is not large at the resonator outlet. This fact can be used for a highly efficient recuperation of the electron energy at the collector. In this respect, the peniotron has advantages over phase-bunching devices such

as O-type TWTs, in which the energy–phase spread of electrons is large and complex and multicascade recuperation systems selecting electrons with different velocities are necessary. As regards the magnetron, it offers no possibility of energy recuperation.

7. Nonsynchronous interaction of relativistic electron flows with the fields of irregular waveguides in superpower microwave electronic devices

The content of this section is based on Refs [45, 46]. The electrodynamic systems of modern high-power and superpower electronic devices (gyrotrons; relativistic traveling- and backward-wave tubes, TWTs and BWTs), including energy leads-in and leads-out, are segments of irregular waveguides. They typically operate in multiwavelength regimes. The characteristics of superpower microwave devices can be improved, first and foremost, by optimizing the profile of their electrodynamic systems. In turn, this requires developing an adequate theory of and computational techniques for arbitrary irregular waveguides.

The technique based on mapping an arbitrary irregular inner surface of the waveguide onto a regular cylinder, coaxial, etc., with a circular or rectangular cross section [47–51] appears to be the most efficient procedure for calculation of irregular waveguides, in terms of both computations and interpretation of the obtained results. In the transformed (oblique) coordinate system, the solution can be written in the form of coupled normal modes using a projection procedure. The amplitudes of the coupled waves are therefore determined by a system of ordinary differential equations with variable coefficients whose form depends on the profile of the nonuniform waveguide. The boundary conditions for this system are specified at the initial and end cross sections of the irregular-waveguide segment (a two-point problem).

If only propagating waves are considered, this problem can be solved using traditional methods without substantial difficulties. As we show in what follows, an accurate calculation of the waveguide also requires accounting for supercritical waves associated with the propagating waves, which substantially modify the properties of the waveguide. But a numerical solution of the (two-point) boundary value problem for supercritical waves cannot be based on traditional (stepwise Runge–Kutta or Hamming) techniques because of their fast divergence (small errors lead to dramatically growing solutions). In this case, an analytic solution should be constructed on a set of given meshpoints so as to satisfy the boundary conditions and decompose the sought functions with respect to a special basis that ensures the solvability of the system of algebraic equations for the decomposition coefficients. For this, we use a block-matrix double-sweep method [52, 53], which differs from the previously suggested double-sweep techniques [54–56]. We also compare the results based on the newly developed technique with those obtained for the same irregularities in the waveguide using a finite-element method.

In addition, we note that the second-kind (Floquet) periodicity condition does not apply to matched segments of periodic irregular waveguides; in view of this, some studies in the theory of TWTs and BWTs [57–60], based on this condition and on the resulting pattern of spatial field harmonics, do not prove to be tenable.

7.1 Self-consistent equations of a nonlinear model of a relativistic BWT and O-type TWT with a slow-wave structure in the form of a corrugated waveguide

The theory of relativistic O-type TWTs and BWTs with electrodynamic systems in the form of irregular corrugated waveguides was developed using the coordinate-transformation method in Refs [47–49, 53, 61]. For a TWT or BWT with a working wave E_{0m} in a hollow irregular waveguide, in the one-dimensional approximation, it yields a system of self-consistent nonlinear equations for the amplitudes of the excited waves:

$$\frac{d\dot{A}_{sm}}{dT} = L_0 (sW\dot{V}_{sm} + v_{0m}\dot{C}_{sm}), \quad (49)$$

$$\frac{d\dot{V}_{sm}}{dT} = -sW \left\{ L_0 \dot{A}_{sm} + \frac{v_{01}^2}{L_0} \left(\frac{dg}{dT} \right)^2 \times \left[\dot{A}_{sm} \frac{1}{3} \left(1 + \frac{4}{v_{0m}^2} \right) + \sum_{k \neq m} \frac{4(v_{0m}^2 + v_{0k}^2)}{(v_{0m}^2 - v_{0k}^2)^2} \frac{J_1(v_{0k})}{J_1(v_{0m})} \dot{A}_{sk} \right] - v_{01}^2 g \frac{dg}{dT} \left(-\frac{\dot{C}_{sm}}{v_{0m}} + \sum_{k \neq m} \frac{2v_{0k}}{v_{0m}^2 - v_{0k}^2} \frac{J_1(v_{0k})}{J_1(v_{0m})} \dot{C}_{sk} \right) \right\}$$

$$- \frac{jsW\sigma r_0}{\pi e_{0m} g} \frac{dg}{dT} \frac{1}{N} \sum_{i=1}^N J_1 \left(\frac{v_{0m}}{v_{01}} \frac{r_0}{g} \right) \exp(-jsW\theta_i);$$

$$\dot{C}_{sm} = -\frac{v_{0m}\dot{V}_{sm}}{(sW)^2 v_{01} g^2} + \frac{1}{L_0 g} \frac{dg}{dT} \times \left(-\frac{\dot{A}_{sm}}{v_{0m}} + \sum_{k \neq m} \frac{2v_{0m}}{v_{0k}^2 - v_{0m}^2} \frac{J_1(v_{0k})}{J_1(v_{0m})} \dot{A}_{sk} \right) - \frac{j\sigma}{sW\pi e_{0m} v_{01}^2 g^2} \frac{1}{N} \sum_{i=1}^N J_0 \left(\frac{v_{0m}}{v_{01}} \frac{r_0}{g} \right) \exp(-jsW\theta_i).$$

The equations of motion of large particles are

$$\frac{d\beta_i}{dT} = -\frac{L_0 E_{zi}}{\beta_i \gamma_i^3}, \quad \frac{d(W\theta_i)}{dT} = \frac{WL}{s\beta_i}, \quad i = 1, \dots, N, \quad (50)$$

$$E_{zi} = \text{Re} \left[\sum_{s=1}^S \sum_{m=1}^M J_0 \left(\frac{v_{0m}}{v_{01}} \frac{r_0}{g} \right) \dot{C}_{sm} \exp(jsW\theta_i) + \frac{r_0}{Lv_{01}g^2} \frac{dg}{dT} \sum_{s=1}^S \sum_{m=1}^M J_1 \left(\frac{v_{0m}}{v_{01}} \frac{r_0}{g} \right) \dot{A}_{sm} \exp(jsW\theta_i) \right], \quad (51)$$

where $T = z/L$, L is the total length of the interaction region, s is the number of the reference-frequency harmonic ω_0 , $W = \omega/\omega_0$, ω is the working frequency, m is the radial index of the E_{0m} wave, v_{0m} is the m th node of $J_0(x)$, $k_0 = \omega_0/c$, $b(T) = k_0 b_v(T)$, $b_v(T)$ is the inner radius (profile) of the waveguide, $g = b(T)/v_{01}$, $L_0 = k_0 L$, $r_0 = k_0 r_e$, r_e is the radius of the tubular electron beam,

$$\dot{A}_{sm} = \frac{b_v \dot{E}_{rsm} e}{m_0 c^2}, \quad \dot{C}_{sm} = \frac{\dot{E}_{zsm} e}{\omega_0 m_0 c}, \quad \dot{V}_{sm} = \frac{b_v \dot{B}_{\phi sm} e}{m_0 c},$$

e and m_0 are the charge and rest mass of the electron, c is the speed of light in the vacuum, $\sigma = 0.73 \times 10^{-3} |I_0|$, I_0 is the beam current in amperes, $\beta_i = v_i/c$, v_i is the velocity of the i th large particle, $\gamma_i = (1 - \beta_i^2)^{-1/2}$, and $e_{0m} = J_1^2(v_{0m})/2$.

We note that excitation equations (49) include both the vortical and the potential (produced by the volume charge)

component of the total field at the frequency $s\omega_0 W$. We additionally clarify this fact. Applying the divergence operation to both sides of the first Maxwell equation yields

$$\operatorname{div} \operatorname{rot} \mathbf{H} = \operatorname{div} \left(\frac{\partial \mathbf{D}}{\partial t} + \boldsymbol{\delta} \right).$$

Therefore, in view of the equation $\operatorname{div} \operatorname{rot} \mathbf{H} = 0$, we have

$$\operatorname{div} \left(\frac{\partial \mathbf{D}}{\partial t} + \boldsymbol{\delta} \right) = 0,$$

where $\boldsymbol{\delta}$ is the total vector of the electric current density and \mathbf{D} is the electric displacement vector. Because $\operatorname{div} \boldsymbol{\delta} = -\partial \rho / \partial t$ according to the continuity equations, we find that

$$\frac{\partial}{\partial t} (\operatorname{div} \mathbf{D} - \rho) = 0$$

in the rest frame. For purely time-dependent processes ($\partial / \partial t \neq 0$), we obtain the third Maxwell equation $\operatorname{div} \mathbf{D} = \rho$. Quite similarly, the fourth Maxwell equation for these processes is implied by the second one. Thus, for purely time-dependent processes, the first and second Maxwell equations determine the full (i.e., including both the vortical and potential components) field excited by a source with the current density $\boldsymbol{\delta}$ with properly specified boundary conditions. This conclusion is also fully applicable to excitation equation (49) with the total electric current density $\boldsymbol{\delta}$ specified in the originally formulated problem [47, 53].

In some problems (for example, in the theory of klystrons), it is reasonable to split the sought electric field \mathbf{E} into a vortical and a potential component,

$$\mathbf{E} = \mathbf{E}_1 + \mathbf{E}_2, \quad \operatorname{div} \mathbf{E}_1 = 0, \quad \operatorname{rot} \mathbf{E}_2 = 0.$$

In this case, the problem decomposes into two coupled problems, a dynamical and a quasi-static one [47–49]:

$$\operatorname{rot} \mathbf{H} = \varepsilon_0 \frac{\partial \mathbf{E}_1}{\partial t} + \boldsymbol{\delta}',$$

$$\operatorname{rot} \mathbf{E}_1 = -\mu_0 \frac{\partial \mathbf{H}}{\partial t},$$

$$\mathbf{E}_2 = -\operatorname{grad} \Phi^e, \quad \nabla^2 \Phi^e = -\frac{\rho}{\varepsilon_0},$$

$$\boldsymbol{\delta}' = \boldsymbol{\delta} - \varepsilon_0 \operatorname{grad} \left(\frac{\partial \Phi^e}{\partial t} \right).$$

If such an approach is used, the current density $\boldsymbol{\delta}$ should be replaced with $\boldsymbol{\delta}'$ in Eqns (49). Obviously, this division is not warranted for TWTs, because it requires repeated calculations of the series representing Φ^e , in the quasi-static and dynamical problems (in the excitation equation). It is interesting that the ‘traditional’ TWT theory contains an obvious error: the quasi-static part (the volume-charge field) is calculated separately but $\boldsymbol{\delta}$ is left in the excitation equation instead of $\boldsymbol{\delta}'$ (see formulas (7.07)–(7.11) in Ref. [59]), which definitely contradicts the above implications of the Maxwell equations. As a result, the quasi-static field is taken into account twice in Ref. [59], which entails an error (not the sole one) in Ref. [59] and other studies based on Ref. [59]. The double inclusion of the potential component can easily be noted in Ref. [59] based on the original formula for the E_z field (see Eqn (6.04) in Ref. [59]):

$$E_z = (\mathbf{E}, \mathbf{z}_0), \quad \mathbf{E} = C_s(z) \mathbf{E}_s - \operatorname{grad} \Phi, \quad \operatorname{div} \mathbf{E}_s = 0.$$

The potential part is written as $-\operatorname{grad} \Phi$. But the ‘vortical’ part $C_s \mathbf{E}_s$ also contains a potential component,

$$\operatorname{div} (C_s(z) \mathbf{E}_s) = (\mathbf{E}_s, \operatorname{grad} C_s) + C_s \operatorname{div} \mathbf{E}_s = E_{sz} \frac{dC_s}{dz} \neq 0,$$

in the region of the sources, where $dC_s/dz \neq 0$.

The boundary conditions for system (49) can be formulated as follows:

(1) for an electric flow not modulated at the entry to the electron-flow-interaction region,

$$W\theta_i(0) = \frac{2\pi}{N} (i - 0.5), \quad \beta_i(0) = \beta_0. \quad (52)$$

At the boundaries of the irregular interaction region matched to the regular waveguide, $[dg/dT(0) = dg/dT(1) = 0]$, the following relations are valid:

(2) for propagating E_{0m} waves,

$$W\dot{A}_{sm}(0) + jk_{sm}^e \dot{V}_{sm}(0) = jk_{sm}^e W 2b(0) \dot{e}_{sm}^+, \quad (53)$$

$$-W\dot{A}_{sm}(1) + jk_{sm}^e \dot{V}_{sm}(1) = jk_{sm}^e W 2b(1) \dot{e}_{sm}^-;$$

(3) for supercritical E_{0m} waves,

$$W\dot{A}_{sm}(0) + k_{sm}^e \dot{V}_{sm}(0) = k_{sm}^e W 2b(0) \dot{e}_{sm}^+, \quad (54)$$

$$-W\dot{A}_{sm}(1) + k_{sm}^e \dot{V}_{sm}(1) = k_{sm}^e W 2b(1) \dot{e}_{sm}^-,$$

where

$$k_{sm}^e = \sqrt{\left| (sW)^2 - \left(\frac{v_{0m}}{g v_{01}} \right)^2 \right|},$$

and \dot{e}_{sm}^+ and \dot{e}_{sm}^- are the relative amplitudes of the forward and backward propagating and supercritical waves at the regular segments matched to the interaction region.

The profile of the irregular corrugated waveguide was specified as

$$b(T) = b_0 + h_v(T) \sin^2 \left(n_v \pi (T + D_v(T)) \right), \quad (55)$$

where $T = (z - z_0)/L_v$, with z_0 and L_v being the entry to and the length of the irregular segment, n_v is the number of periods, $h_v(T)$ is the depth of corrugations, $D_v(T)$ is the function specifying the period variation, $D_v(0) = 0$, $D_v(1) = 0$, and the period at $D_v(T) = 0$ is constant and equal to $d = k_0 L_v / n_v$ in the accepted units.

We approximate the functions $h_v(T)$ and $D_v(T)$ by a series in shifts of the standard finitary function $\varphi_3(x)$ that represents the third-power B spline [54],

$$h_v(T) = \sum_{k=1}^K h_k^v \varphi_3 [T(K-3) - k + 2], \quad (56)$$

$$D_v(T) = \sum_{k=1}^K d_k^v \varphi_3 [T(K+3) - k - 1],$$

$$\varphi_3(x) = \begin{cases} 0, & |x| \geq 2, \\ \frac{(2-x)^3}{6}, & 1 \leq x \leq 2, \\ \frac{1}{6} [1 + 3(1-x) + 3(1-x)^2 - 3(1-x)^3], & 0 \leq x \leq 1, \\ \varphi_3(-x), & x \leq 0. \end{cases}$$

We note that the coefficients n_k and d_k in this approximation respectively correspond to the values of the functions $h_v((k-2)/(K-3))$ and $D_v((k+1)/(K+3))$.

The efficiency of the interaction is determined by the following relations:

(1) in terms of the power of the waves excited by the flow (the ‘wave’ efficiency),

$$\eta_{sm}(T) = \pi e_{0m} \frac{\text{Im} [\dot{A}_{sm}(T) \dot{V}_{sm}^*(T) - \dot{A}_{sm}(0) \dot{V}_{sm}^*(0)]}{(\gamma_0 - 1) \sigma},$$

$$\eta_s^v = \sum_m \eta_{sm}^v; \quad (57)$$

(2) in terms of the kinetic energy loss by the electron flow (the ‘electron’ efficiency),

$$\eta^e(T) = \frac{1}{N} \sum_{i=1}^N \frac{\gamma_0 - \gamma(T)}{\gamma_0 - 1}. \quad (58)$$

The phase bunching of the electrons is determined by the bunching function

$$G_r(T) = \frac{1}{N} \left[\left(\sum_{i=1}^N \cos sW\theta_i \right)^2 + \left(\sum_{i=1}^N \sin sW\theta_i \right)^2 \right]^{1/2}. \quad (59)$$

If the energy exchange is weak, G_r is close to the relative first harmonic of the beam current.

7.2 Special features of calculations of supercritical waves

It can be seen from Eqn (51) that the exact solution for the full electromagnetic field of the frequency sW in the waveguide under consideration can in general be written as an infinite series in m . Over an extended interval without sources, this expansion has only a finite number of terms, which represent traveling normal-mode waves E_{0m} with indices $1 \leq m \leq m_p$ (where m_p is the number of subcritical waves for a given radius b). All supercritical waves decay over a sufficiently long regular interval. To obtain the exact solution in representation (51) for the irregular interval or for a regular interval with sources, several supercritical E_{0m} waves with indices $m_p < m \leq m_e = M$ must be taken into account along with the traveling waves (here, m_e is the number of supercritical waves taken into account).

A specific feature of the boundary value problem for system of differential equations (49) is that direct numerical calculations based on a shooting method, with supercritical waves included, are unstable because of the presence of exponentially increasing components in the representation of the general solution, i.e., the Cauchy problem is ill-posed. To solve such problems, directional-orthogonalization techniques [55] and various versions of the differential double-sweep method [52, 56] were previously suggested, but they have only limited applicability. In the context of solving this boundary value problem, we here consider a universal stable algorithm based on the block-matrix double-sweep method. We write the system of differential equations for complex amplitudes (49) in the standard form

$$\frac{d\mathbf{u}}{dT} = G(T) \mathbf{u} + \mathbf{f}(T), \quad (60)$$

$$\mathbf{u} = \{u^1, \dots, u^{2M}\}$$

$$= \{\dot{A}_1, \dot{V}_1, \dot{A}_2, \dot{V}_2, \dots, \dot{A}_m, \dot{V}_m, \dots, \dot{A}_M, \dot{V}_M\},$$

$$\mathbf{f} = \{f^1, f^2, \dots, f^{2M-1}, f^{2M}\}. \quad (61)$$

The elements of the complex matrix G of size $2M$ were obtained by combining like terms in system (49) according to representation (61); they are functions of T . The link with the equations of motion is realized through the vector $\mathbf{f}(T)$, which includes the terms of Eqns (49) containing σ .

We specify the boundary conditions for Eqn (60) using Eqns (53) and (54) in the general form

$$\alpha_m^0 u^{2m-1}(0) + \beta_m^0 u^{2m}(0) = \gamma_m^0,$$

$$\alpha_m^L u^{2m-1}(1) + \beta_m^L u^{2m}(1) = \gamma_m^L, \quad m = 1, \dots, M. \quad (62)$$

To numerically solve the boundary value problem in (60) and (62), we choose a uniform mesh $\{T_i = (i-1)h, h = 1/n, i = 1, \dots, n+1\}$; here, $\{\mathbf{u}_i = \mathbf{u}(T_i)\}$ is the table of the values of the sought solution at the meshpoints. For computations, we use the third-order, three-point implicit finite-difference Adams scheme,

$$\frac{\mathbf{u}_{i+1} - \mathbf{u}_i}{h} = \frac{5}{12} (G\mathbf{u} + \mathbf{f})_{i+1}$$

$$+ \frac{8}{12} (G\mathbf{u} + \mathbf{f})_i - \frac{1}{12} (G\mathbf{u} + \mathbf{f})_{i-1}. \quad (63)$$

We note that this scheme yields a three-diagonal block matrix with a predominant diagonal element. By collecting like terms in Eqn (63), we obtain the following system of algebraic equations (if we ignore the \mathbf{u} dependence of \mathbf{f}):

$$\frac{h}{12} G_{i-1} \mathbf{u}_{i-1} - \left(E + \frac{8h}{12} G_i \right) \mathbf{u}_i + \left(E - \frac{5h}{12} G_{i+1} \right) \mathbf{u}_{i+1} = \mathbf{d}_i, \quad (64)$$

where

$$\mathbf{d}_i = \frac{h}{12} (5\mathbf{f}_{i+1} + 8\mathbf{f}_i - \mathbf{f}_{i-1}), \quad i = 2, \dots, n,$$

and E is the unit matrix. System (64) should be supplemented with the missing second-order finite-difference equation

$$\frac{\mathbf{u}_2 - \mathbf{u}_1}{h} = \frac{G_1 \mathbf{u}_1 + f_1 + G_2 \mathbf{u}_2 + f_2}{2} \quad (65)$$

and the boundary conditions

$$\alpha_m^0 u_1^{2m-1} + \beta_m^0 u_1^{2m} = \gamma_m^0, \quad \alpha_m^L u_n^{2m-1} + \beta_m^L u_n^{2m} = \gamma_m^L. \quad (66)$$

To solve the system of linear equations (64)–(66) with a band matrix, we developed an economical modification of the Gauss method, the block-matrix double-sweep method.

The solution of self-consistent system of equations (60) can be obtained as the result of the following iteration process. First, system (60) is solved at the given boundary conditions and at $\mathbf{f}^0 = 0$. Next, equations of motion (50) are solved for the E_z fields determined from formula (51), and $\tilde{\mathbf{f}}^1$ is found, after which iterations are repeated to reach convergence. For the iterations, we use the sequential lower relaxation,

$$\mathbf{f}^{k+1} = \omega_r \tilde{\mathbf{f}} + (1 - \omega_r) \mathbf{f}^k, \quad \omega_r = 0.1 - 0.6.$$

In our notation, the dimensionless components E_r , E_z , and B_φ of the symmetric wave E fields of the cylindrical longitudinally irregular waveguide at the fundamental frequency

$s = 1$ can be obtained from the solution of the boundary value problem

$$\begin{aligned} \dot{B}_\phi &= \frac{u(r, z)}{r}, & \dot{E}_r &= \frac{j}{W} \frac{1}{r} \frac{\partial u}{\partial z}, \\ \dot{E}_z &= -\frac{j}{W} \frac{1}{r} \frac{\partial u}{\partial r}, & u(z, r) &= u_{re} + ju_{im}. \end{aligned}$$

In the region $0 \leq r \leq b(z)$ and $0 \leq z \leq L$,

$$\frac{\partial}{\partial z} \left(\frac{1}{r} \frac{\partial u}{\partial z} \right) + \frac{\partial}{\partial r} \left(\frac{1}{r} \frac{\partial u}{\partial r} \right) + \frac{W^2}{r} u = 0. \quad (67)$$

The boundary conditions are as follows:

$$\text{at } r = 0, \quad u = 0;$$

at the conducting boundary $[r = b(z), \partial u / \partial \mathbf{n} = 0$, where \mathbf{n} is the vector normal to the surface],

$$\text{at } z = 0, \quad -\frac{\partial u}{\partial z} + jk_m^e u = e^+ r J_1(v_{0m} r)$$

(an incident E_{0m} wave);

$$\text{at } z = L, \quad \frac{\partial u}{\partial z} + jk_m^e u = 0$$

(the condition of perfect matching for the E_{0m} wave).

The power passing through the cross section is

$$\begin{aligned} P &= \text{Re} \int_0^{b(z)} E_r B_\phi^* r dr \\ &= \frac{1}{W} \int_0^{b(z)} \left(u_{im} \frac{\partial u_{re}}{\partial z} - u_{re} \frac{\partial u_{im}}{\partial z} \right) \frac{dr}{r}. \end{aligned} \quad (68)$$

Test computations. To check the accuracy of the proposed Galerkin technique, we solved the problem of the reflection of an E_{01} wave in the regular cylindrical waveguide of radius b_0 from a nonuniformity of the form of sinusoidal grooves of depth h and width d ,

$$b(z) = \begin{cases} b_0, & z < z_1, \\ b_0 + h \sin^2 \frac{\pi(z - L_1)}{d}, & z_1 \leq z \leq z_1 + kd, \\ b_0, & z_1 + kd < z < L. \end{cases}$$

The values of z_1 and L were chosen such that the supercritical waves excited on the surface decay and only the E_{01} wave of the regular waveguide is observed at the cross sections $z = 0$ and $z = L$. Figure 17 presents the depth (h) dependences of the ratio of passing power (68) to the passing power of the regular waveguide. Curves 1 were obtained using a Galerkin technique with eight basis functions, and curves 2 from the solution of the boundary value problem using the method of triangular finite elements with the MATLAB package. We chose $z_1 = 1.5b_0$ and $L = 2z_1 + kd$. The region was divided into 2750 elements. If the number of elements is 4000, the curves coincide in all graphs, i.e., the results based on the finite-element method converge to the results obtained using the Galerkin method.

Violation of the second-kind periodicity condition in matched segments of periodic waveguides. The violation of this condition was already noted in [53, 61–63] in both the general case (EH_{nm} - and HE_{nm} -waves [61]–[63]) and the case of E_{0m} -waves considered here [52]. These inferences were confirmed by calculation results for matched segments of periodic corrugated E_{0m} -mode waveguides obtained by

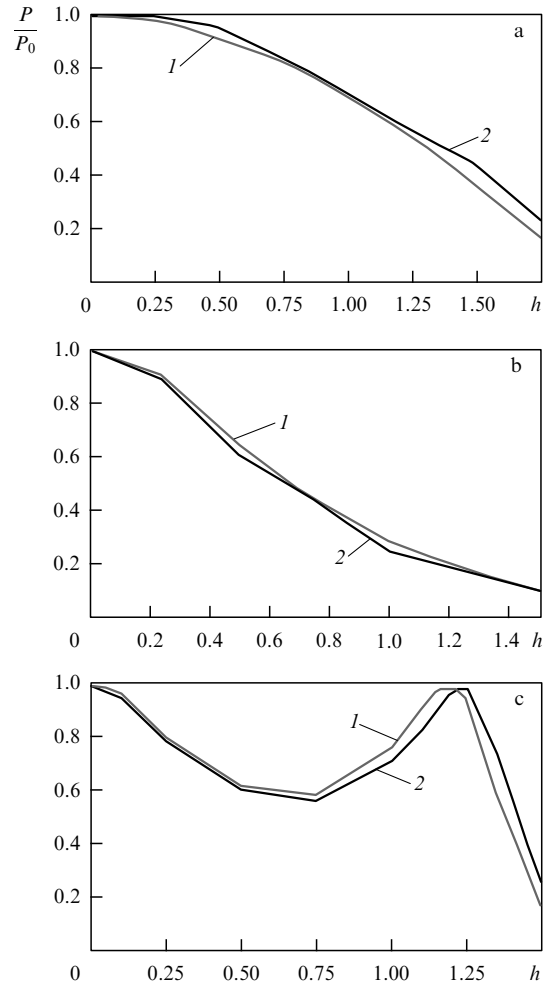


Figure 17. Dependences of the passing power on the groove depth h for $d = 2$: (a) $b_0 = 3, k = 1$; (b) $b_0 = 2.5, k = 1$; (c) $b_0 = 2.5, k = 2$.

solving problem (67) using both the finite-difference and Galerkin methods. Figures 18a and 18b present the contour maps of the function $\text{Re} [r \dot{B}_\phi(r, z)]$ computed using the finite-difference method for two waveguide configurations (these lines are close to \mathbf{E} field lines). Figure 19 illustrates the variation of the modulus of the longitudinal component $|\dot{E}_z(r_0, z)|$ along a segment of a corrugated waveguide, calculated using the Galerkin method. We note that an accurate computation of such a waveguide using a finite-difference method can hardly be carried out because of the insufficient performance of modern personal computers. It can be seen from Figs 18 and 19 that the distributions of both $r \dot{B}_\phi$ and \dot{E}_z over the corrugated segment are not periodic in either case. As noted previously in Refs [51, 52, 61–63], this conclusion is important for the formulation of an adequate self-consistent theory of TWTs and BWTs. In view of this inference, the theories based on the consideration of “synchronous spatial harmonics of the field” in the slow-wave structure of a BWT or TWT are erroneous. This can be particularly emphasized in the case of Ref. [60]; the author of that study neglects the transversal and longitudinal boundary conditions for a piecewise-periodic corrugated structure and considers ‘spatial harmonics’ using their Fourier transform.

Calculation and optimization of a relativistic corrugated-waveguide-based generator. We use self-consistent system (49)–(51) with boundary conditions (52)–(54) and apply

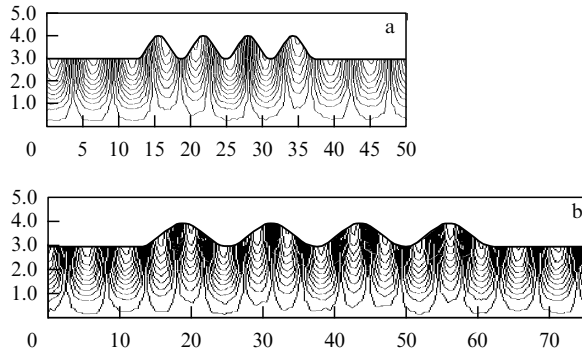


Figure 18. Contours of $\text{Re}[u(r, z)]$ obtained using the finite-difference method: (a) $b_0 = 3, h = 1, d = 2\pi$ (b) $b_0 = 3, h = 1, d = 4\pi$.

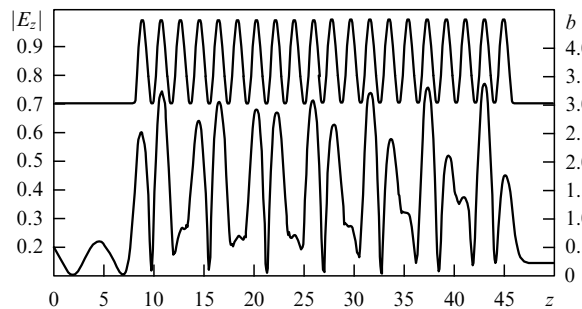


Figure 19. Variation of the modulus of the E_z wavefield component along a segment of the corrugated waveguide at $b_0 = 3$ and $d = 1.9$ at the level $r_0 = 2.5$.

the block-matrix double-sweep method to calculate the following arrangement of the three-wave generator with an optimized corrugation profile: $b_0 = 9.5, r_0 = 9, h = 1.3, d = 1, \beta_0 = 0.79$ ($U_0 = 320$ kV) $I_0 = 1$ A, and $\eta_e = 0.56$.

The variation in the corrugation period $D_v(z)$ is specified by the coefficients $d_{\text{var}} = d_{1-6}$ [see Eqns (55) and (56)], where the d_{1-6} are respectively equal to 0.003, 0.035, $-0.012, -0.053, 0.082$, and -0.01 .

Figure 20 presents the variations in the characteristics of the interaction in this case. Curves 4–6 correspond to wave efficiencies (57) for the E_{01}, E_{02} , and E_{03} waves, respectively. In this case, the electron efficiency is 13% higher than in the corresponding case with a regular corrugation. A higher efficiency is achieved at a low bunching degree due to the prolonged confinement of the bunch at the braking phase of the $(E_{02} + E_{03})$ -wave superposition. In contrast, the E_{01} wave yields the energy gained as E_{02} and E_{03} are converted into E_{01} at the irregularities of the corrugated waveguide: the phase speed of this wave increases (the corrugation period increases), and therefore the bunch finds its way to the accelerating phase of the wave.

It is remarkable that the power yielded by the electrons is transferred to both the exit and entry, and the powers transferred to the left and to the right at the entry are equal in this case: $P^-(0) \simeq P^+(0)$; at the same time, a nearly perfect matching is realized at the exit: $P^-(1) \simeq 0; P^+(1) \simeq P(1)$ (Fig. 20b). This suggests that as the waves are reflected at the entry, this arrangement is effectively an internal-feedback generator. The variation in the phase increase of the ‘hot’ wave, $\varphi = \arctan(E_{z\text{im}}/E_{z\text{re}})$ at $r = r_0$, shown in Fig. 20c, indicates that the wave travels oppositely to the motion of the

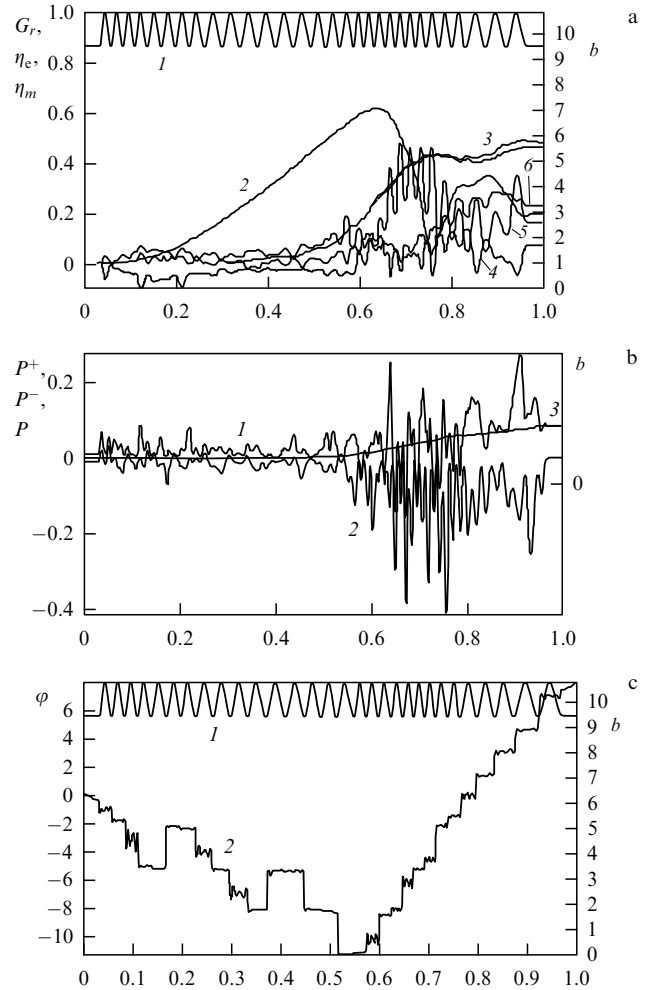


Figure 20. Characteristics of the chosen arrangement of the three-wave generator: (a) 1, $b(T)$; 2, $G_r(T)$; 3, η_e ; 4, η_1 ; 5, η_2 ; 6, η_3 ; (b) 1, P^+ ; 2, P^- ; 3, P ; (c) 1, $b(T)$; 2, $\varphi(T)$.

electrons in the first half of the interaction region. The bunching of the beam then increases monotonically without energy removal from it. The energy removal increases sharply at the end, where the phase of the wave begins increasing and, accordingly, the energy transfer becomes mainly concurrent with the motion of the electrons toward the end of the region. The slope of the $\varphi(T)$ curve at the end section corresponds to the deceleration of the hot wave, $\beta_{\text{ph}}^h \approx 0.73$. We note that in most cases of regular or irregular TWTs (either single-mode or dual-mode) that we analyzed using the efficiency optimization, we observed the above-described regime of nonsynchronous interaction.

Acknowledgments. We are grateful to Yu V Gulyaev and V I Pustovoi for useful discussions.

References

1. Kolomenskii A A, Lebedev A N *Dokl. Akad. Nauk SSSR* **145** 1259 (1962) [*Sov. Phys. Dokl.* **7** 745 (1963)]
2. Davydovskii V Ya *Zh. Eksp. Teor. Fiz.* **43** 886 (1962) [*Sov. Phys. JETP* **16** 629 (1963)]
3. Kuraev A A, Shevchik V N *Radiotekh. Elektron.* **9** 1083 (1964)
4. Kuraev A A *Sverkhvysokochastotnye Pribory s Periodicheskimi Elektronnyimi Potokami* (Microwave Devices with Periodic Electron Flows) (Minsk: Nauka i Tekhnika, 1971)

5. Kuraev A A, Sinitsyn A K, Shcherbakov A V *Radiotekh. Elektron.* **44** 891 (1999) [*J. Commun. Technol. Electron.* **44** 833 (1999)]
6. Petelin M I *Izv. Vyssh. Uchebn. Zaved. Radiofiz.* **17** 902 (1974) [*Radiophys. Quantum Electron* **17** 686 (1974)]
7. Bratman V L et al., in *Relyativistskaya Vysokochastotnaya Elektronika* (Relativistic High-Frequency Electronics) Issue 1 (Gor'kii: Inst. Prikl. Fiz., Akad. Nauk SSSR, 1979) p. 157
8. Bratman V L et al. *Int. J. Electron.* **51** 541 (1981)
9. Bratman V et al. *IEEE J. Quantum Electron.* **QE-19** 282 (1983)
10. Ginzburg N S, Zarnitsyna I G, Nusinovich G S *Izv. Vyssh. Uchebn. Zaved. Radiofiz.* **24** 481 (1981) [*Radiophys. Quantum Electron* **24** 331 (1981)]
11. Bratman V L, Denisov G G, Ofitserov M M, in *Relyativistskaya Vysokochastotnaya Elektronika* (Relativistic High-Frequency Electronics) Issue 3 (Gor'kii: Inst. Prikl. Fiz., Akad. Nauk SSSR, 1983) p. 127
12. Bratman V L, Novozhilova Yu V, Sergeev A S *Izv. Vyssh. Uchebn. Zaved. Radiofiz.* **30** 1261 (1987)
13. Bratman V L, Denisov G G, Lukovnikov D A *Izv. Vyssh. Uchebn. Zaved. Radiofiz.* **33** 976 (1990) [*Radiophys. Quantum Electron.* **33** 718 (1990)]
14. Eremka V D, Zhurakhovskii V A, Kovalenko A M *Dokl. Akad. Nauk Ukr. SSR, Ser. A: Fiz.-Mat. Tekh. Nauki* (10) 63 (1990)
15. Dikun T F et al. *Radiotekh. Elektron.* **29** 293 (1984)
16. Kuraev A A, Sinitsyn A K *Radiotekh. Elektron.* **30** 1794 (1985)
17. Kurayev A A, Sinitsyn A K, Slepyan A Ya *Int. J. Electron.* **80** 603 (1996)
18. Botvinnik I E et al. *Pis'ma Zh. Eksp. Teor. Fiz.* **35** 418 (1982) [*JETP Lett.* **35** 511 (1982)]
19. Botvinnik I E et al. *Pis'ma Zh. Eksp. Teor. Fiz.* **8** 1386 (1982) [*JETP Lett.* **8** 596 (1982)]
20. Bogachenkov V A et al. *Kratk. Soobshch. Fiz. FIAN* (6) 38 (1983)
21. Kuraev A A, Popkova T L *Dokl. Nats. Akad. Nauk Belarusi* **42** 120 (1998)
22. Kuraev A A, Sinitsyn A K *Radiotekh. Elektron.* **43** 468 (1997) [*J. Commun. Technol. Electron.* **43** 434 (1997)]
23. Vainshtein L A *Osnovy Sverkhvysokochastotnoi Elektroniki* (Foundations of Superhigh-Frequency Electronics) Pt. 2 (Saratov: Saratov. Gos. Univ., 1970) p. 84
24. Kapitza P L *Usp. Fiz. Nauk* **44** 7 (1951)
25. Miller M A *Izv. Vyssh. Uchebn. Zaved. Radiofiz.* **1** 110 (1958)
26. Miller M A *Izv. Vyssh. Uchebn. Zaved. Radiofiz.* **1** 166 (1958)
27. Zhurakhovskii V A, Orlov N N, Chemeris V T, Preprint No. 261 (Kiev: Inst. Energetiki Akad. Nauk USSR, 1981)
28. Kuraev A A, Sinitsyn A K *Radiotekh. Elektron.* **32** 1686 (1987)
29. Kolosov S V, Kuraev A A *Radiotekh. Elektron.* **18** 2558 (1973)
30. Kuraev A A, Sinitsyn A K *Radiotekh. Elektron.* **42** 214 (1997) [*J. Commun. Technol. Electron.* **42** 194 (1997)]
31. Kalinin V I, Gershtein G M *Vvedenie v Radiofiziku* (Introduction to Radiophysics) (Moscow: Gostekhizdat, 1957) p. 513
32. Levellin F B *Inertsiya Elektronov* (Inertia of Electrons) (Moscow: Gostekhizdat, 1946)
33. Shevchik V N *Osnovy Elektroniki Sverkhvysokikh Chastot* (Foundations of Superhigh-Frequency Electronics) (Moscow: Sov. Radio, 1959)
34. Gaiduk V I, Palatov K I, Petrov D M *Fizicheskie Osnovy Elektroniki Sverkhvysokikh Chastot* (Physical Foundations of Superhigh-Frequency Electronics) (Moscow: Sov. Radio, 1971) p. 116
35. Kuraev A A, Sinitsyn A K, Shcherbakov A V *Radiotekh. Elektron.* **50** 491 (2005) [*J. Commun. Technol. Electron.* **50** 456 (2005)]
36. Ono S et al. "Cyclotron fast tube utilizing spatial harmonic interaction. Travelling-wave peniotron. Pt. 1. Theoretical analysis", *Sci. Rep. V.B.-14. No. 2* (Tohoku: Res. Inst. Tohoku Univ., 1962) p. 49
37. Golenitskii I I, Eremka V D, Sazonov V P "Elektrovakuumnye istochniki millimetrovykh i submillimetrovykh voln na garmonikakh tsiklotronnoi chastoty" ("Vacuum-tube sources of millimeter and submillimeter waves based on harmonics of the cyclotron frequency", in *Obzory po Elektronnoi Tekhnike* (Reviews of Electronics) Ser. 1 *Elektronika SVCh* (Superhigh-Frequency Electronics) Issue (Moscow: Tsentr. Nauchno-Issled. Inst. 'Elektronika', 1988)
38. Kuraev A A *Radiotekh. Elektron.* **35** 1278 (1990)
39. Kuraev A A, Paramonov B M, Sinitsyn A K *Radiotekh. Elektron.* **40** 102 (1995)
40. Kuraev A A, Matveenko V V, Sinitsyn A K *Radiotekh. Elektron.* **39** 1661 (1994)
41. Eremka V D et al. *Radiotekh. Elektron.* **45** 357 (2000) [*J. Commun. Technol. Electron.* **45** 329 (2000)]
42. Shcherbakov A V, in *Sbornik Nauchnykh Rabot* (Collection of Scientific Works) Ch. 1 (Kharkiv, 1999) p. 217
43. Ishihara T et al. *IEEE Trans. Electron Dev.* **46** 798 (1999)
44. Sukhorukov A P et al. *Vestn. Mosk. Gos. Univ. Ser. 3, Fiz. Astron.* (3) 15 (2000) [*Moscow Univ. Phys. Bull.* **55** (3) 11 (2000)]
45. Kravchenko V F, Kuraev A A, Sinitsyn A K *Elektromagn. Volny Elektron. Sist.* **10** 44 (2005)
46. Kravchenko V F et al. *Dokl. Ross. Akad. Nauk* **404** 470 (2005) [*Phys. Dokl.* **50** 483 (2005)]
47. Kuraev A A *Izv. Akad. Nauk Belorues. SSR, Ser. Fiz.-Tekh. Nauk* **1** 121 (1979)
48. Kuraev A A *Teoriya i Optimizatsiya Elektronnykh Priborov SVCh* (Theory and Optimization of Microwave Electronic Devices) (Minsk: Nauka i Tekhnika, 1979)
49. Kuraev A A *Moshchnye Pribory SVCh. Metody Analiza i Optimizatsii Parametrov* (High-Power Microwave Devices: Methods of Analysis and Optimization of Parameters) (Moscow: Radio i Svyaz', 1986)
50. Kuraev A A *Izv. Nats. Akad. Nauk Belarusi. Ser. Fiz.-Tekh. Nauk* (4) 60 (1999)
51. Kuraev A A, Sinitsyn A K *Elektromagn. Volny Elektron. Sist.* **7** (3) 12 (2002)
52. Batura M P, Kuraev A A, Sinitsyn A K, in *Materialy 14-i Mezhdunar. Konf. "SVCh Tekhnika i Telekommunikatsionnye Tekhnologii"* (Proc. 14th Intern. Conf. "Microwave and Telecommunication Technologies") (Sevastopol', 2004) p. 175
53. Batura M P et al. *Dokl. Belaruss. Gos. Univ. Informatiki Radioelektron.* (4) 26 (2004)
54. Marchuk G I, Agoshkov V I *Vvedenie v Proektionno-setochnye Methody* (Introduction to Projection-Mesh Techniques) (Moscow: Nauka, 1981)
55. Il'inskii A S, Slepyan G Ya *Kolebaniya i Volny v Elektrodinamicheskikh Sistemakh s Poteryami* (Oscillation and Waves in Electrodynamical Systems with Losses) (Moscow: Izd. MGU, 1983)
56. Bugaev S P et al., in *Relyativistskaya Vysokochastotnaya Elektronika* (Relativistic High-Frequency Electronics) Issue 5 (Gor'kii: Inst. Prikl. Fiz., Akad. Nauk SSSR, 1988) p. 78
57. Silin R A, Sazonov V P *Zamedlyayushchie Sistemy* (Slow-Wave Systems) (Moscow: Sov. Radio, 1966)
58. Solntsev V A, Romashin N L, Kravchenko N P, in *Lektsii po Elektronike SVCh i Radiofizike: 8-ya Zim. Shkola-Seminar Inzhenerov* (Lectures on Superhigh-Frequency Electronics and Radiophysics: 8th Winter School-Seminar for Engineers) Vol. 1 (Saratov: Izd. Saratov. Univ., 1989) p. 5
59. Vainshtein L A, Solntsev V A *Lektsii po Sverkhvysokochastotnoi Elektronike* (Lectures on Superhigh-Frequency Electronics) (Moscow: Sov. Radio, 1973)
60. Solntsev V A *Radiotekh. Elektron.* **43** 1285 (1998) [*J. Commun. Technol. Electron.* **43** 1193 (1998)]
61. Kolosov S V, Kuraev A A *Elektromagn. Volny Elektron. Sist.* **4** 44 (1999)
62. Kuraev A A, Navrotskii A A, Sinitsyn A K *Elektromagn. Volny Elektron. Sist.* **8** (1) 4 (2003)
63. Kurayev A A, Sinitsyn A K, Yaromenok S I, in *4th IEEE Intern. Conf. on Vacuum Electronics, Seoul, Korea, 28-30 May 2003* (Piscataway, NJ: IEEE, 2003) p. 225